UNIVERSITY OF OKLAHOMA

GRADUATE COLLEGE

Evaluation of the Madden-Julian Oscillation and the Stratospheric Polar Vortex and Their Joint Influence on the Northern Hemisphere Extratropical Circulation

A THESIS

SUBMITTED TO THE GRADUATE FACULTY

in partial fulfillment of the requirements for the

Degree of

MASTER OF SCIENCE IN METEOROLOGY

By

Matthew Robert Green
Norman, Oklahoma
2018

Evaluation of the Madden-Julian Oscillation and the Stratospheric Polar Vortex and Their Joint Influence on the Northern Hemisphere Extratropical Circulation

A THESIS APPROVED FOR THE
SCHOOL OF METEOROLOGY

BY

Dr. Jason C. Furtado, Chair

Dr. Naoko Sakaeda

Dr. Steven Cavallo

Acknowledgments

The research that is presented within this thesis would not have been possible without the support and leadership of my advisor, Dr. Jason Furtado. Under his guidance, I have learned how to become a well rounded researcher and student. During the last two years, Dr. Furtado has shown me how to ask important questions and to be a critical thinker. With the experience and the opportunities of the Master's research provided by Dr. Furtado, I am motivated to continue to build my educational and research skills through pursuing a PhD in atmospheric science.

Along with Dr. Furtado, my committee has shown great support and guidance through our many discussions. Dr. Naoko Sakaeda and Dr. Steven Cavallo have used their backgrounds and experiences to aid in my Master's research. They offered different perspectives to grow and diversify the research project.

There have been many people outside of this committee that have supported me along my journey as a graduate student. Establishing a support system is very important when moving and adjusting to a new place like Oklahoma. Elisa, Brian, Joel, Addison, and Matt Flournoy are only a few of the many people that have been critical in building a home in Norman. I would especially like to thank Briana for her ability to keep me strong through her strength and encouragement as I completed this thesis. Thank you to all of these people, and many more, for their support through thick and thin.

Finally, I would like to thank my family for their everlasting support as I moved 1,319 miles away from home to pursue my dreams. Robert, Elizabeth, and Jeffrey have given guidance and love throughout my educational career, giving me the courage and strengthen to complete this Master's work. Thank you to everyone that has impacted my life and put me on course to complete this thesis.

Table of Contents

List of Tables

List of Figures

Abstract

Multiple modes of climate variability inform long-range Northern Hemisphere (NH) winter weather prediction through their interactions with the atmosphere. Two specific modes of variability that are the focus of this study are: (1) the state of the stratospheric polar vortex (SPV) and (2) the Madden-Julian Oscillation (MJO). The stratospheric polar vortex is a phenomenon whose variability can influence the NH polar jet stream. The MJO's enhanced tropical convection can perturb Rossby waves that propagate poleward, vertically, and zonally along the jet stream, interacting with the extratropical atmosphere. While these climate modes and their influence on winter weather patterns have been studied separately, their joint relationship and its interaction with the wintertime extratropical circulation remains undetermined.

This study analyzes the combined influence of the NAM_{100} and the MJO on NH subseasonal to seasonal winter weather patterns. Using the ERA-Interim dataset, the study analyzes a series of conditional composites of outgoing longwave radiation (OLR) MJO index (OMI) during neutral SPV state, strong/weak SPV during weak OMI, and joint OMI and SPV events. Neutral state of the SPV and weak state of the MJO refer to event that occur when these indices have very low amplitude. We find that the MJO maintains control of the pattern primarily in the Pacific Basin. The SPV, on the other hand, has a stronger influence on tropospheric patterns over the North Atlantic and Europe. Extended-range predictability of weather patterns over the Eastern US, for example, could result in significant forecast error if only using the SPV as a predictor compared to using both the MJO and the state of the SPV together. Analyzing the joint composite also produces signals of constructive and destructive interference between these two modes. For example, when the OMI is in phases 7 & 8 (7 & 8) during weak (strong) SPV, strong constructive (destructive) interference results, with enhanced positive height anomalies over the Arctic and strong annular negative anomaly pattern.

Dynamical analysis of propagating waves, using Eliassen-Palm (EP) flux, show stratosphere-troposphere interactions change with the influence of the MJO-SPV relationship. OMI 7,8 (2,3,4) and SPV events are observed to increase (decrease) the anomalous upward propagation of Rossby waves into the stratosphere. Through the composite analysis it is assumed that the two modes work independently of one another to influence extratropical patterns. However, we investigate whether this assumption holds true, analyzing the MJO's influence on the stratosphere-troposphere relationship. Our results show that during the period of composite analysis (+10-14 days after event) the MJO influences patterns most strongly in the troposphere. Through observing the changes in the NAM through the stratosphere and troposphere, OMI 7,8 (2,3,4) during neutral SPV influence negative (positive) changes in the NAM index upward through the troposphere and into the stratosphere. These OMI events during neutral SPV events do not depict the initiation of stratospheric events, showing a lack of downward propagation of the anomalous NAM signal into the troposphere.

This study provides an understanding of the processes of the MJO-SPV relationship to improve S2S forecasting for NH extratropical winter weather patterns. OMI and SPV joint events show that, compared to individual events, variability of the weather patterns +10-14 days after events are decreased, thereby potentially increasing the predictability of NH weather patterns on S2S timescales. Implications for climate modeling are also found here, through providing consistent patterns of dynamical processes for model verification. Valuable predictability of S2S weather patterns is available through using only the MJO and the SPV congruently to forecast winter weather patterns in the NH.

Chapter 1

Introduction and Background

Winter weather patterns over the Northern Hemisphere (NH) are influenced by a number of modes of variability. On the sub-seasonal to seasonal timescale (S2S), two particular climate modes of interest are variability associated with the stratospheric polar vortex (SPV) (Waugh et al. 2017) and the Madden-Julian Oscillation (MJO) (Madden and Julian 1971). Although the SPV has a primary circulation in the stratosphere, effects from the changes in its speed and location impact the tropospheric circulation at later times (Baldwin and Dunkerton 2001; Kidston et al. 2015). Likewise, the MJO is associated with convection in the tropical Indian and Pacific Oceans but features teleconnections that affect patterns in the mid- to high-latitudes (Frederiksen and Lin 2013). The current paradigm for S2S forecasting considers the MJO or the SPV, but there could be valuable information in using both of the modes together (e.g., Vitart et al. 2012). This research focuses on the patterns and mechanisms that are observed during combined events of the MJO and the SPV in order to better understand how these modes enhance the reproducibility of winter weather patterns. We first build a foundational understanding of the two modes, beginning with the stratosphere-troposphere dynamics, followed by the MJO. Next, we will look at the connection observed between MJO and other NH climate patterns. Finally, research questions aimed to address the key issues and interests of this study will be discussed.

1.1 Stratosphere-Troposphere Dynamics

Variations in solar radiation throughout the year bring changes in temperature patterns that are observed throughout the atmosphere. Temperature changes in the stratosphere can lead to large circulation variations throughout the year. As solar radiation decreases in the fall, the mean temperature throughout the atmosphere cools at high latitudes. Proportional to

temperature, geopotential heights fall in the regions of decreasing temperature, which increases a north-south oriented height gradient. This gradient is strong at the level of the tropopause. These gradients dynamically control the speed and location of westerly winds associated with the polar jet stream. The southern flank of both the tropospheric and stratospheric polar vortex is marked by this accelerated westerly winds circulations, and they occur in both the NH and Southern Hemispheres (SH) (Kidston et al. 2015).

Important to this research is the understanding of key climate indices used to measure the state of the stratosphere and the troposphere circulation and geopotential height patterns. The Northern Annular Mode (NAM) is a measure of the geopotential heights throughout the atmosphere regressed on to the leading empirical orthogonal function (EOF) and represents the strength of the annular circulation (Baldwin and Dunkerton 2001; Thompson and Wallace 2000). 50 hPa geopotential height regression map associated with the NAM 50 hPa level is displayed in Figure 1.1b (Thompson and Wallace 2000). The Arctic Oscillation (AO) is defined as the NAM index at 1000 hPa and corresponds to the changes in geopotential height at this level (Baldwin and Dunkerton 1999). The regression map associated with this mode of variability is shown in Figure 1.1d (Thompson and Wallace 2000). The North Atlantic Oscillation (NAO) is another diagnostic for tropospheric impacts, measuring the sea level pressure dipole in the North Atlantic. Positive NAO is observed as positive height anomalies. Also using an EOF method for developing the principle component time series, a positive NAO is represented by anomalous negative geopotential heights over Iceland with anomalous high heights over the Azores, while a negative NAO exhibits the opposite anomalous pattern (Feldstein 2003). These tools allow for a more accurate way to quantify and diagnose that patterns of the atmosphere.

The SPV is the stratospheric part of the polar vortex circulation and is most variable during the boreal winter (Baldwin and Dunkerton 2001). The SPV is categorized by two types of NAM events, weak and strong. Using the NAM, a generalized weak event is when the NAM less than or equal to -1.0σ_{NAM} (anomalously positive height anomalies over pole),

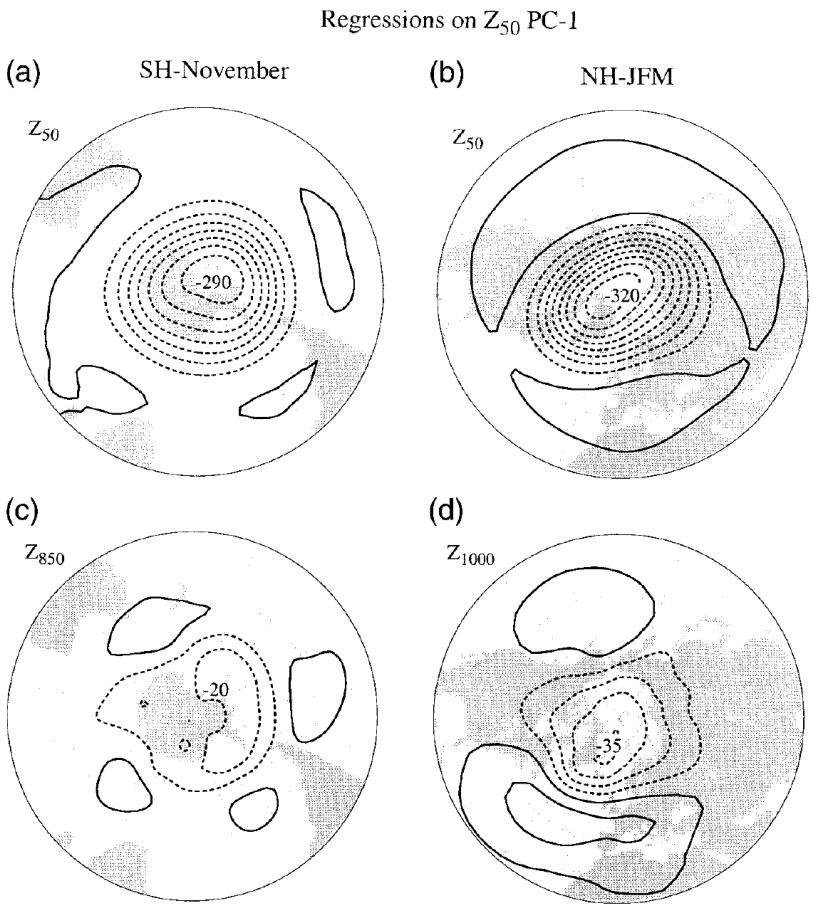

Figure 1.1: Geopotential height (meters) regression maps onto the leading principal component time series. (Top) Regression maps for 50 hPa GPH level for SH (November) and NH (January - March). (Bottom) Regression maps for 850 hPa (SH) and 1000 hPa (NH) levels. Contour intervals is 40m for 50 hPa maps, and 10 m for 850 hPa and 1000 hPa maps. From Thompson and Wallace (2000).

while a generalized strong event is when NAM greater than or equal to $+1.0\sigma_{NAM}$ (anomalously negative height anomalies over pole). Here, σ_{NAM} represents the standardized values of NAM index, further discussed in Chapter 2. A strong SPV event is characterized by anomalously strong westerly wind that is more contracted toward the pole. A weak event is characterized by anomalously weak westerly winds. More extreme cases of a weakened SPV (i.e., sudden stratospheric warmings (SSWs)) can take two forms. One form features

the circulation that is weakened and the vortex displaced from the pole, while the second form features a circulation that is weakened so dramatically that the zonal wind reverses and becomes easterly. These are characterized by minor and major SSWs, respectively (Limpasuvan et al. 2004). Once an event occurs within the upper stratosphere, the effect can last for approximately 30 days (Baldwin and Dunkerton 2001). Wave propagation that initiates these stratospheric events originate in the troposphere and dynamically influence the circulation of the stratosphere.

Vertically propagating Rossby waves into the stratosphere break and deposit easterly acceleration onto the climatological westerly wind (Haynes 2005; Thompson et al. 2006). Meridional and vertical wave propagation can be assessed through the use of Eliassen-Palm (EP) flux (Edmon Jr. et al. 1980), which is represented by:

$$\mathbf{F} = \left\{F_{(y)}, F_{(p)}\right\}, \tag{1.1}$$

where

$$F_{(y)} = -\overline{v'u'}, \tag{1.2}$$

$$F_{(p)} = f\overline{v'\theta'}/\overline{\theta}_p. \tag{1.3}$$

In Equations 1.1 - 1.3 above, the overbar and prime notation represents that zonal mean and departures from the mean, u and v are the zonal and meridional velocities, y denotes the north-south coordinate, $f = f(y)$ is the Coriolis parameter, p represents the vertical pressure coordinate, θ is potential temperature, and $\overline{\theta}_p$ represents that partial derivative with respect to pressure, effectively measuring the static stability. Flux measured using equation 1.2 is proportional to northward easterly momentum. Equation 1.2 is inversely proportional to meridional transport of zonal momentum. Hence, positive $F_{(y)}$ represents northward transport of easterly momentum. In the case of the SPV, waves with a meridional divergence of $F_{(y)}$ component will act to deposit easterly momentum onto the circulation through waves breaking, forcing it to decelerate. Westerly momentum is then transported toward lower latitudes. Equation 1.3 is proportional to meridional heat transport. Thus,

vertically propagating waves ($F_{(p)} > 0$) will deposit heat in the polar stratosphere (Edmon Jr. et al. 1980). The divergence of the EP-flux also assists in determining how the wave propagation will impact the existing circulations. Given by:

$$\nabla \cdot \mathbf{F} = \frac{\partial F_{(y)}}{\partial y} + \frac{\partial F_{(p)}}{\partial p} \tag{1.4}$$

In the quasi-geostrophic approximation, the linearized governing equations show that EP-flux divergence is proportional to the change of mean zonal flow with time. Therefore, in regions of observed divergence of EP-flux, an acceleration of the westerlies is expected. Conversely, convergence of EP-flux leads to a deceleration of the westerly circulation (Edmon Jr. et al. 1980). This is observed as a direct impact on the SPV and is a focus of this research.

Observing wave propagation through EP-flux allows for the life cycle of stratospheric events to be more efficiently analyzed. Limpasuvan et al. (2004) analyzed the life cycle of the SSWs through the use of these fluxes. They found that prior to the weakening of the SPV, waves propagate upward into the climatological westerlies. Represented by EP-flux convergence, waves break due to their inability to propagate through easterlies or strong westerly winds (Haynes 2005). Through continued upward propagation of Rossby waves, the critical level (marking the level of wave breaking and anomalous easterly zonal-mean zonal wind) continues to lower, forcing vertically propagating waves to break at lower altitudes. Therefore, the level of anomalous easterly circulation continues to lower through downward control of the stratosphere through the inhibition of vertical propagating Rossby waves (Haynes et al. 1991). With limited accessibility of Rossby waves to propagate into the upper stratosphere, wave breaking is decreased in the stratosphere. A resulting acceleration of the stratospheric westerlies is accompanied by equatorward momentum flux, which forces a residual circulation to for air to rise over the polar cap, cooling the layer and lowering geopotential heights. Strengthening the north-south temperature and height

gradients, the residual circulation further encourages the acceleration of the stratospheric polar vortex (Kidston et al. 2015).

Downward control of wave processes through the stratosphere onto the troposphere subsequently influences strength and position of the tropopsheric circulation (Haynes et al. 1991). Thompson et al. (2006) also found that the persistence and amplitude of the tropospheric response to the change in the stratosphere are a balance between the stratospheric wave drag and radiative heating anomalies. These changes in the troposphere can have large latitudinal extent and are observed throughout the entire depth of the troposphere (Thompson and Wallace 2000). Examples of these changes are seen through impacts to the position of storm tracks over the NH, equator-shifted for weak events and pole-shifted pattern for strong events, resulting in a greater potential for extreme cold air outbreaks during weak vortex events (Baldwin and Dunkerton 2001; Kidston et al. 2015; Waugh et al. 2017).

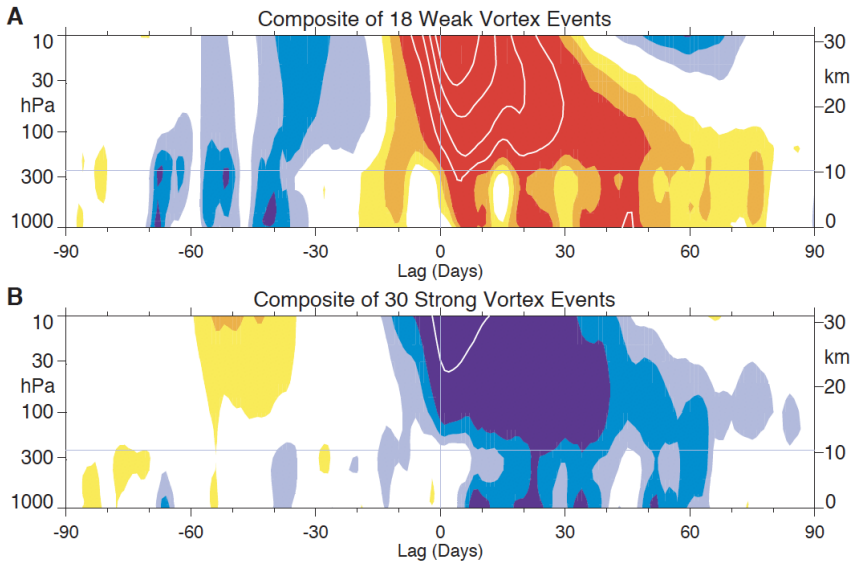

Figure 1.2: Time-height composites of the Northern Annular Mode index. (A) 18 weak vortex events and (B) 30 strong vortex events are defined using the 10 hPa level respectively for index values that cross -3.0 and +1.5. From Baldwin and Dunkerton (2001).

Stratosphere-troposphere coupling introduces increased predictability of tropospheric weather patterns through the state of the stratosphere. Upper tropospheric responses to

changes in the stratosphere directly impact surface patterns, such as that of the Arctic Oscillation (AO). In Figure 1.2, the NAM index is plotted for -90 to +90 days around a stratospheric polar vortex event. Baldwin and Dunkerton (2001) categorized the weak events as when the 10 hPa NAM $\leq$ -3.0σ and strong events when the 10 hPa NAM $\geq$ +1.0σ. These events were chosen so that an event initiated at this level may be strong enough to reach the troposphere. Figure 1.2 indicates that the timescale for an event lasting in the stratosphere (p $\leq$ 250 hPa) is on the order of 30-60 days. In the troposphere, an oscillatory pattern is observed, with the anomalous NAM signal of vortex events lasting greater than 60 days. Furthermore, note that the stratospheric anomalies in the NAM lead the tropospheric changes in the NAM. The implication from this figure (Kidston et al. 2015; Waugh et al. 2017) is that changes in the SPV could be used to skillfully predict tropopsheric circulation patterns via downward propagation of stratospheric circulation anomalies. Baldwin et al. (2003) showed that the 150 hPa NAM index was more skillful in predicting the surface based AO monthly pattern than the AO's skill in predicting itself, both given 10 day leads. These studies show that the stratospheric pattern is important for adding predictive skill for tropospheric weather patterns in the winter season (Baldwin et al. 2003; Waugh et al. 2017).

As mentioned earlier, the SPV can influence different tropospheric weather regimes depending on the phase. Extreme weather events are most closely related to changes in the tropospheric polar vortex (Waugh et al. 2017). These changes come in increased amplitudes of troughs and ridges that impact the meridional extent of the tropospheric polar vortex. Cold-air outbreaks are some of the most frequent extreme events during the winter season, as troughs in the polar vortex move anomalously cold air to the south (Waugh et al. 2017). Linked to cold-air outbreaks, increased atmospheric blocking during weakened vortex events can lead to changes in the positioning of storm tracks and anomalous precipitation (Kidston et al. 2015). However, these changes are not consistent from one vortex event to another, and they are especially not consistent from the NH to the SH. As

the NAM weakens severely and the center of the vortex is displaced from the pole, temperature patterns in the Eastern and Western Hemispheres are very different (Kidston et al. 2015).

The processes in the SH differ in comparison to the NH. When the Southern Annular Mode (SAM) is strengthened, loss of ozone in the stratosphere is associated colder than average temperatures over Antarctica, while temperature in southern South America are higher than average. Precipitation over the mid-latitudes of the Southern Hemisphere increase in southeastern Australia and the Southern Alps of New Zealand is associated with a weakening of the SAM. Weakening of westerly flow in the Southern Hemisphere, consistent with the NAM, is associated with a weakening of the SAM (Thompson and Wallace 2000; Haynes 2005; Kidston et al. 2015). Although the SAM has similar processes to the NAM, the circulation is less variable throughout much of the year and is rarely completely easterly (Thompson and Wallace 2000). Changes occurring during its active season of the month of November are still initiated through wave-mean flow interactions and is dynamically similar to that of the NAM (Barnes and Hartmann 2010). However, the focus of this study will be placed on the impacts and changes of the NH circulation.

1.2 Madden-Julian Oscillation

The MJO represents variability of the tropical circulation and convection that propagates eastward through the Indian and western/central Pacific Oceans over 30-90 days (Zhang 2005). Originally discovered by Madden and Julian (1971, 1972), the MJO was observed not only to have local effects, but also impact circulation patterns on a global scale. Interaction with extratropical patterns occur as a result of a Rossby wave train, originating from regions of enhanced convection of the MJO (e.g. Matthews et al. 2004; Moore et al. 2010; Roundy 2012). The Real-time MJO Monitoring Index (RMM) is a commonly used MJO index, which categorizes the MJO into eight phases, the particular phase of the convection depends location of decreased outgoing longwave radiation, as well as the wind patterns

throughout the troposphere. Spanning from the western Indian Ocean to the central Pacific Ocean, the location of the convection is characterized by RMM phases 1-8 (Zhang 2005). Analyzing convection throughout the Indian Ocean, as well as the western to central Pacific Ocean, this research focuses on two RMM phase groups 2,3,4 and 7,8. The reasoning for the construction of these groups is discussed in Chapter 2. Although the MJO affects circulation patterns in both the NH and SH, this research analyzes its influence on the NH winter weather patterns.

Figure 1.3 displays the winds and circulations that help to control and are a result of enhanced MJO convection. Divergence of the 200 hPa winds and convergence of the 850 hPa winds are collocated with regions of enhanced convection. Regions of suppressed convection are collocated with convergence of 200 hPa winds and divergence of 850 hPa winds (Hendon and Salby 1994). At 200 hPa, winds above the enhanced convection are easterly, as there resides an anticyclonic circulation to the north and south. At 850 hPa, a cyclonic anomaly is observed to the north and south of this region, as the convection is associated with westerlies (Rui and Wang 1990).

The upper-level circulation that results from the tropical heating and the 200 hPa wind pattern are responsible for changes in circulation patterns downstream of enhanced convection. As the enhanced convection propagates to the east, the circulation pattern follows the region of convection. As the enhanced convection dissipates, the upper-level patterns continue to propagate to the east to modulate downstream patterns within the tropics and the extratropics (Rui and Wang 1990). North of the upper tropospheric anticyclone circulation, associated with the enhanced convection, 200 hPa westerly winds are accelerated. North of suppressed convection, the cyclonic convection acts to decelerate the westerly winds. Acceleration of winds directly impacts the location and strength of the Asian-Pacific Jet. Enhanced convection located within the Indian Ocean acts to retract and accelerate the jet over south-central Asia. An extension and acceleration of the jet located over the western

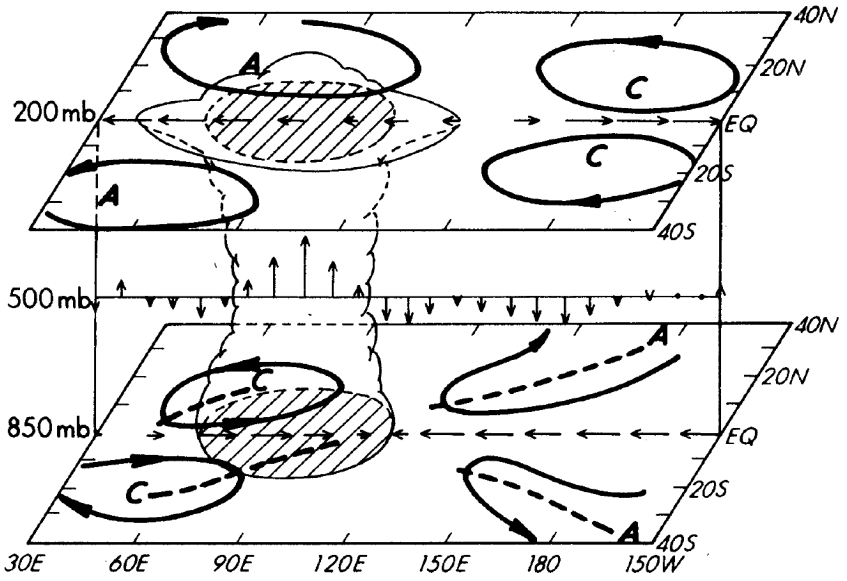

Figure 1.3: Schematic depicting the characteristic structure of low-frequency waves on intraseasonal time-scale representative of phase 3 of the MJO. A and C represent anticyclonic and cyclonic circulations, respectively. Vertical and zonal wind is shown through vectors plotted at 500 mb, 200 and 850 mb. From Rui and Wang (1990).

and central Pacific, occurs with enhanced convection located in this region of the Pacific (Matthews et al. 2004; Moore et al. 2010).

Rossby wave response to the tropical heating originates from the upper-level wave pattern north of enhanced convection. The positioning of Asian-Pacific jet impacts anticyclonic and cyclonic wave breaking in the North Pacific. The northern flank of the northward shifted jet is conducive of a baroclinic zone that encourages wave breaking and extratropical surface cyclone formation in the North Pacific (Moore et al. 2010). Propagation of Rossby waves downstream influences wave patterns on the global scale. Wave patterns and geopotential height anomalies over North America are influenced by this teleconnection interaction. Positive height anomalies over eastern North America are associated with convection in the Indian Ocean. Opposite patterns occur with convection located within the central Pacific (Madden and Julian 1994).

1.3 Northern Hemisphere Circulation interactions with the MJO

Several studies have analyzed the interaction between the MJO and the NH extratropical climate modes, such as the Pacific-North American pattern (PNA), the AO, and the NAO. L'Heureux and Higgins (2008) found that early phases of the RMM (2,3,4) were associated with a positive AO tendency, while later phases of the RMM (7,8) were more associated with a tendency toward negative AO (shown in Fig. 1.4). Zhou and Miller (2005) find this same relationship but through wave patterns in the North Pacific connecting the two climate modes. Lin et al. (2009) show MJO convection positioned in the Indian Ocean was found to be associated with a lagged positive NAO pattern, while Pacific MJO convection was associated with a lagged negative NAO. Geopotential heights anomalies over North America, represented by the PNA, have also been observed to be influenced by the location of MJO convection. Frederiksen and Lin (2013) found that phase 4 most strongly promoted a negative PNA signal across North America. Henderson et al. (2016) also found that negative PNA, a pattern associated with increased European blocking occurred prior to MJO phase 6.

The MJO also interacts with the stratosphere processes. Jiang et al. (2017) found when preceding joint events of the NAO and the MJO, wave propagation into the stratosphere is either decreased for positive NAO events given a MJO or increased for negative NAO events given MJO events. A lack of wave propagation led to NAO signals that were short lived in comparison to when there was preceding wave propagation into the stratosphere. Garfinkel et al. (2012, 2014) discovered that a major SSW event occurs approximately 30+ days after RMM phase 3, while 13-24 days after phase 7 a major SSW event occurs. This shows that a long lag of RMM phase 3 and relatively shorter lag of phase 7 have the same relationship with the stratospheric patterns. These significant results give evidence to the MJO being used for enhanced prediction of the stratospheric pattern on a sub-seasonal timescale, relative to the predictability of SSWs without the MJO relationship. By way of enhanced predictability of SSWs using the MJO, tropospheric patterns resulting from this stratospheric

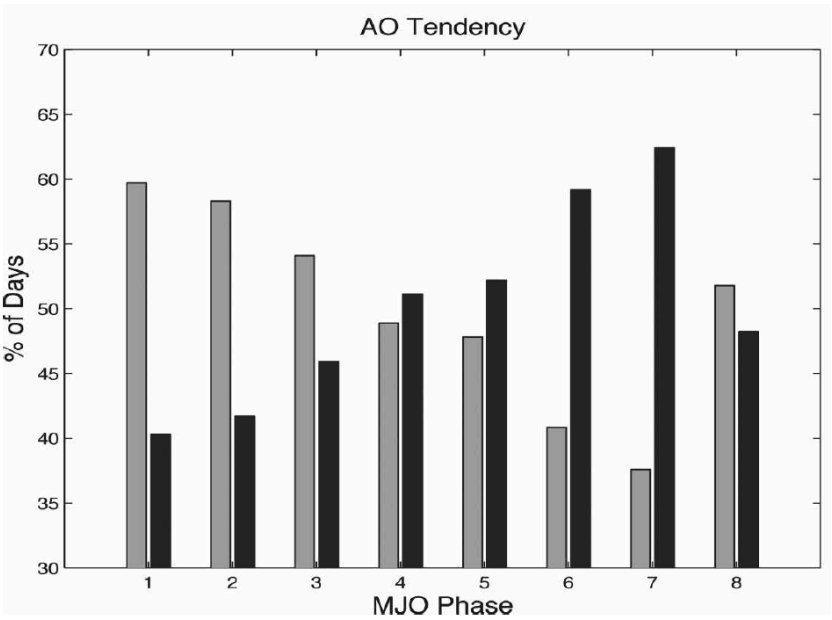

Figure 1.4: Percentage of MJO days (phases defined using Wheeler and Hendon (2004) criteria) that have a positive (gray) or negative (black) Arctic Oscillation index tendency. 10-day running mean filter was applied to the AO index. From L'Heureux and Higgins (2008).

state also increase in predictability (Schwartz and Garfinkel 2017). As discussed earlier, this is a result of the downward control of wave propagation and stratosphere-troposphere coupling. Wang et al. (2018) shows through dynamical wave analysis that during frequent occurrence of phase 4 events of the RMM, downward wave propagation led to enhanced divergence in the stratosphere. The opposite phenomenon occurred during phase 7, with strong upward wave flux into the stratosphere.

1.4 Research Questions

Little focus has been placed on the interaction of the MJO and both states of the stratosphere, as both weak and strong SPV regimes influence tropospheric patterns. This study seeks to better understand the relationship between the MJO and the SPV to diagnose their

joint influence on the NH extratropical patterns on a S2S timescale. This increased understanding may be used in the future to improve predictability of the weather impacts. Fueling this study are four research questions, aimed to more completely understand this relationship.

1. What are the specific weather patterns that are controlled by the MJO and the SPV separately? How do these observations change during combined events?

2. For combined events of the MJO and SPV on the S2S timescale, how do extratropical weather patterns change in the Northern Hemisphere?

3. Does the variability of extratropical weather patterns decrease when the MJO and SPV occur together rather when they are apart?

4. Do the MJO and the state of the SPV work independently of one another to influence weather patterns, or are they acting on the other through dynamical interactions?

    (a) Does the MJO influence weather patterns through influencing the stratospheric pattern first, or are they influenced strictly via tropospheric teleconnection?

Based upon previous studies (Garfinkel et al. 2012, 2014; Schwartz and Garfinkel 2017; Wang et al. 2018), there is a relationship between the MJO and the SPV that helps to encourage particular extratropical patterns in the NH. It is with this information that we hypothesize that such a relationship will add information to the weather patterns and improve consistency of the weather patterns during joint events. Through their separate dynamical processes, there will be cases in which the MJO and SPV work to strengthen patterns, while other cases act to destroy particular patterns. This should provide inference that is observed when comparing the joint events to the MJO-only and SPV-only composites. Providing answers to these questions will allow for a more in depth comprehension of the processes at work during the interaction of the MJO and the SPV and their impact on tropospheric weather patterns.

The thesis is organized as follows. A discussion of the data and methodology used for this study is explored in Chapter 2. Chapter 3 focuses on the patterns found in the composite analysis results. Chapter 3 continues with the impact of this relationship on extreme weather patterns by the change of the blocking regimes. Chapter 4 investigates the impact of the MJO onto the stratosphere through analysis of wave dynamics. Chapter 5 concludes with a discussion and summary.

Chapter 2

Methodology

2.1 Data

This study uses 39 years (1979-2017) of daily data from the European Centre for Medium-Range Weather Forecasts (ECMWF) Re-Analysis Interim dataset (Dee et al. 2011). Using a horizontal resolution of 1.5^o x 1.5^o with a vertical resolution of 23 pressure levels from the 1000 hPa to 1 hPa, atmospheric parameters such as 500 hPa geopotential height (GPH), 250 hPa zonal wind, and surface air temperature (SAT) are analyzed. The ERA-Interim's vertical resolution and extent, allows for a large portion of the stratosphere to be analyzed, which is the reason why it is specifically used for this study (Dee et al. 2011). EP flux is used for wave propagation analysis and is derived from Edmon Jr. et al. (1980). The focus of this study is on the months of October - March, to analyze the influence of the MJO and the SPV on cold season weather extremes in the NH. This season is also the active season for stratosphere-troposphere coupling (Thompson and Wallace 2000; Kidston et al. 2015). The anomalies constructed in this study use a 30-year (1981-2010) average of the daily values. The anomalies are then linearly detrended to avoid the influence of climate change on temporal statistics.

The MJO is defined using the Outgoing Longwave Radiation (OLR) MJO Index (OMI) (Kiladis et al. 2014), and is obtained from the Earth System Research Laboratory[1]. This index uses solely OLR to measure the convection in the tropics to quantify the state of the MJO, compared to the Wheeler and Hendon (2004) RMM index which uses 200 hPa and 850 hPa winds as well as OLR to measure the MJO (Straub 2013). The RMM method has the potential to initialize MJO events from the wind pattern alone, whereas the OMI pattern initializes events from the MJO convection directly. The phase and amplitude are derived

[1] https://www.esrl.noaa.gov/psd/mjo/mjoindex/

from this index in a similar manner set forth by Wheeler and Hendon (2004). Compared to the Wheeler and Hendon (2004) Real-time Multivariate Mode (RMM) method for finding the MJO characteristics, the OMI only uses a 20-96 day filtered OLR projection onto the daily spatial patterns of the empirical orthogonal function (EOF) of the 30-96 day eastward filtered OLR (Kiladis et al. 2014). The projection of the OLR onto the first and second leading EOFs provide two principal component (PC) timeseries. In the Kiladis et al. (2014) methodology, the negative of the OMI (PC1) corresponds to Wheeler and Hendon (2004) RMM (PC2), and OMI (PC2) corresponds to the RMM (PC1). The order and sign of the OMI PC time series used in a manner as to compare directly to the phase and amplitude of the RMM. Using this framework, phase and amplitude of an MJO event are found as follows:

$$phase = tan^{-1}(-OMI(PC1)/OMI(PC2)) \tag{2.1}$$

$$amplitude = \sqrt{OMI(PC2)^2 + (-OMI(PC1))^2} \tag{2.2}$$

A phase space (Figure 2.1) is used to divide the index into eight unique phases, marking the location of the MJO associated active and suppressed convection (Wheeler and Hendon 2004). This diagram also allows enhanced convection to be tracked in time. From hereon, events of the MJO will be labeled as OMI phases 2,3,4 and 7,8 to more accurately represent the response to the MJO convection.

When using the OMI to categorize the position and strength of the MJO, there are a few caveats that must be considered. When projecting observations onto the OMI PCs, other features of tropical convection might influence the index. Roundy et al. (2009) found that Kelvin waves can project onto the RMM PCs, and its contribution to the value of the index cannot be neglected. Equatorial Rossby waves can also contribute to the signal if the MJO pattern is associated with these waves. ENSO patterns can also influence the categorization of the MJO. During El Niño, MJO patterns can project onto parts of the third leading PC, which is not considered when finding the MJO's amplitude and phase (Kessler

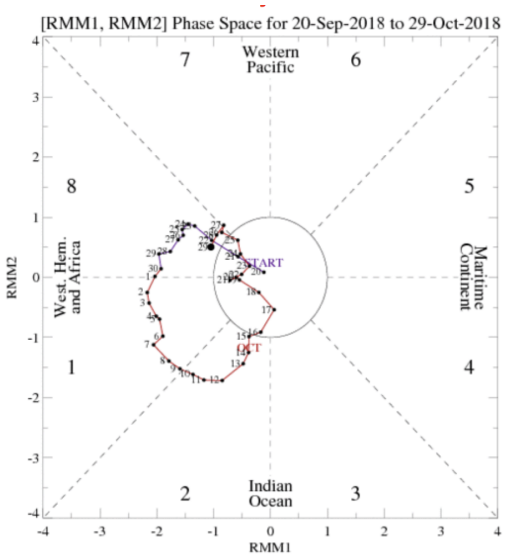

Figure 2.1: [RMM1,RMM2] phase space points for dates of 20-Sept-2018 through 29-Oct-2018 (Dated line), represents phase and amplitude of the MJO enhanced convection. Eight regions as defined by Wheeler and Hendon (2004) are labeled with associated regions. Unit circle (MJO amplitude ≤ 1.0) represents weak MJO. Figure from Climate Prediction Center (`http://www.cpc.ncep.noaa.gov/products/precip/CWlink/MJO/whindex.shtml`).

2001). Although the OMI is chosen to more accurately represent the positioning of the MJO convection, there are still factors that must be accounted for when using the index to categorize the MJO.

The NAM in this study is defined as the leading EOF of the GPH at each pressure level from the ERA-Interim reanalysis (Baldwin and Dunkerton 2001). The timeseries of the NAM index is then the leading PC timeseries for those levels. For this study, the 100 hPa level PC is used to define the events of the SPV. This level is being used to capture stratospheric events that are most likely to propagate down into the troposphere. Conclusions of the study are robust (albeit with some different events) when using 50 hPa to define events for compositing (not shown).

2.2 Composite Analysis

To better understand the MJO and the SPV and its impacts on the winter weather patterns in the NH, many different atmospheric parameters are used to identify key characteristics that both the MJO and the SPV contribute to these patterns. Through the use of composite analysis, 500 hPa GPH anomalies, 250 hPa zonal wind anomalies and SAT anomalies are analyzed for specific combinations of the phases of the OMI and the SPV.

OMI phases 2, 3, and 4 are grouped together, associated with active convection over the Eastern Indian Ocean and the Maritime Continent, and suppressed convection over the Pacific and Western Indian Oceans. Phases 7 and 8 are grouped together, associated with active convection over the dateline and Western Pacific, and suppressed convection over the Indian Ocean and Maritime Continent (Zhang 2005). These phase groups were chosen based on the results of L'Heureux and Higgins (2008), showing these phase groups preferred opposite phases of the surface-based AO. Also, along with the OMI phase groups containing close regions of enhanced convection, the sample size of OMI events is larger. This will help when subdividing the events in the composited cases. For compositing events, σ_{OMI} represent standardized values of the OMI amplitude obtained from Equation 2.2 and σ_{NAM} represents standardized geopotential height anomalies at 100 hPa. A OMI-only event is defined when the OMI amplitude is greater than or equal to $+1\sigma_{OMI}$, while the SPV is in a neutral state($-1.0\sigma_{NAM} \leq \mathrm{NAM}_{100} \leq 1.0\sigma_{NAM}$). The two phases of the SPV are strong ($\mathrm{NAM}_{100} \geq 1.0\sigma_{NAM}$) and weak ($\mathrm{NAM}_{100} \leq -1.0\sigma_{NAM}$) and must occur while the OMI is weak (OMI amplitude $< 1.0\sigma_{OMI}$ for any phase). The SPV is considered neutral when the NAM index at 100 hPa is between $-1\sigma_{NAM}$ and $1\sigma_{NAM}$. The purpose of analyzing these composites for their independent cases is to remove any instantaneous influence that the OMI may be at the start of an SPV event and similarly, any influence that the SPV may have on the patterns at the start of an OMI event.

There are four conditional or joint composite cases we will examine, in addition to the single OMI/SPV composites, denoted by the (+) sign:

- OMI 2,3,4 + weak SPV
- OMI 2,3,4 + strong SPV
- OMI 7,8 + weak SPV
- OMI 7,8 + strong SPV

To analyze these events, within the first five days of the start of a OMI event the SPV must be in one of the three possible scenarios (strong, weak, neutral). The first day that fits this criteria is then used as the start date for each event. After the first day of an event is found, the OMI events must last for at least 3 days at or above the threshold, while the SPV events must last for at least 5 days above their appropriate threshold. This is to make sure that the event has a long enough lifetime to impact extratropical weather patterns. This process is the same for the SPV strong and weak (OMI weak) composites. After the first date of the event, the parameters are then composited by pentads (Pentad 0: Days 0-4; Pentad 1: Days 5-9; and Pentad 2: 10-14). For this study, we will examine results only for Pentad 2 to better understand how the patterns change on the extended weather timescale. Table 2.1 displays the number of start dates that correspond to each of the categorized events. Throughout the period of study, there are a larger number of OMI-only events compared to the SPV-only events. Also, OMI phase 2,3,4 favor a greater number of events combined with the strong SPV, than that of the weak SPV. The opposite is observed for OMI phases 7 and 8. The number of events that correspond to OMI 2,3,4 (weak, strong, and neutral SPV) are greater than that of the OMI 7,8 due to the number of phases included in the analysis. A caveat for categorizing these events, is that a SPV event that propagates down into the troposphere, or has a long lifetime in the stratosphere (30-60 days) can last for multiple OMI phases, if the OMI amplitude is large enough for an event to be composited. However, removing overlapping events, may cause the sample size of the analysis to drop severely. So, any OMI event that has a large coinciding SPV event is composited if it meets the criteria, regardless if separate OMI phases occur during the same SPV event.

Event Count			
	Neut. SPV	Weak SPV	Strong SPV
Weak OMI		37	43
OMI 2,3,4	78	28	27
OMI 7,8	69	18	18

Table 2.1: Number of events for each of the individual and combined cases composited throughout this analysis.

Significance of the composites is found using a method similar to that of Schwartz and Garfinkel (2017), which measures the consistency of the pattern within a composite. If 66% of the events composited agree on the sign of the anomaly, each point where this is observed is marked as significant. Rather than assessing the strength of the anomaly, this study focuses on the consistency and robustness of the anomalous pattern. Similar to Schwartz and Garfinkel (2017), we use this binomial signs test to indicate that the chance of 66% of events will be of any particular sign has a relatively small probability (e.g., $< 9x10^{-4}$ for 100 events).

2.3 Blocking Analysis

Atmospheric blocks are extreme weather events, influencing cold air outbreaks and large deviations in storm tracks and strengths (Berggren et al. 1949). Many other studies have analyzed blocking regimes in the NH to better understand their frequency and also their orientation (e.g. Masato et al. 2012, 2013a,b; Henderson et al. 2016). The position and strength of atmospheric blocks, influences the wind patterns, increasing the anomalous meridional winds around the regions of the blocks. Along with driving storm motion, translated to the surface, these winds drive temperature advection. This study analyzes blocking and how the frequency changes in the NH during the MJO and SPV cases, described in Section 2.2.

Changes in the conditional composites of the MJO and the SPV blocking episode frequency will show how the frequency of extreme weather changes with these patterns as well.

The Tibaldi and Molteni (1990) methodology is adopted to comprehensively analyze blocking over the entire NH. 500 hPa GPH anomalies (Z) are used for the blocking analysis. Analyzed from 40.5^{o}N to 60^{o}N, the blocking index for the is latitude band is built using:

$$BI = \frac{Z(\phi_o) - Z(\phi_s)}{(\phi_o - \phi_s)} \tag{2.3}$$

where

ϕ_o = 60^{o}N + Δ,

ϕ_s = 40.5^{o}N + Δ,

Δ = -3^o, 0^o or 3^o .

A particular longitude is considered blocked at a specific time if at least one of the Δ conditions satisfies BI > 0. Tibaldi and Molteni (1990) methodology also has a northern blocking index (60^{o}N to 80^{o}N), but they acknowledge that a block with large southward extent would not satisfy the northern blocking criteria. Therefore, like them, we define blocks using only the BI equation. Significant difference from the blocking frequency climatology was found using Monte Carlo testing of 5000 iterations with a confidence interval of 0.9, in order to obtain a relatively large sample size.

Chapter 3

Composite Analysis of the MJO and the SPV

The focus of this chapter is to understand of the patterns that result from MJO and SPV interactions. By using 500 hPa GPH anomalies, 250 hPa zonal wind anomalies, and SAT anomalies, upper air patterns as well as sensible impacts at the surface are observed. Investigating the independent MJO-only and SPV-only composites first will show patterns resulting from their individual influence. Here, the MJO and the SPV maintain strong relationships with the patterns of particular regions, while also working to interfere with each other, producing patterns not observed in their independent composites.

3.1 500 hPa Geopotential Height Anomaly Composite Analysis

First we examine how MJO-SPV interaction may influence atmospheric wave patterns across the NH. Figure 3.1 displays day +10 to +14 composites of boreal cold season 500 hPa geopotential height anomalies (GPHa) for the independent and joint events of the MJO and the SPV. For weak SPV + weak OMI (Fig. 3.1a) events, a large area of positive GPHa exists over the Arctic while an annular pattern of negative anomalies surround the Arctic in the mid-latitudes. The strong SPV + weak OMI events show a pattern that has similar orientation, but opposite sign to that of the weak SPV (compare Fig. 3.1b to Fig. 3.1a). These patterns agree well with the patterns found by Thompson and Wallace (2000). For both weak and strong SPV events, pattern consistency exists over the Arctic and North America. However, in the case of the weak SPV (Fig. 3.1a), significant anomalies are found over the North Pacific and East Asia, whereas the strong SPV (Fig. 3.1b) cases are associated with a greater area of significance in the North Atlantic and parts of Europe. A smaller area of significance observed in the weak SPV (Fig. 3.1a) case is most likely a result of the

variability in the location of the positive GPHa that occurs when the SPV breaks down and weakens, leading to a decrease in the consistency of the pattern in this region.

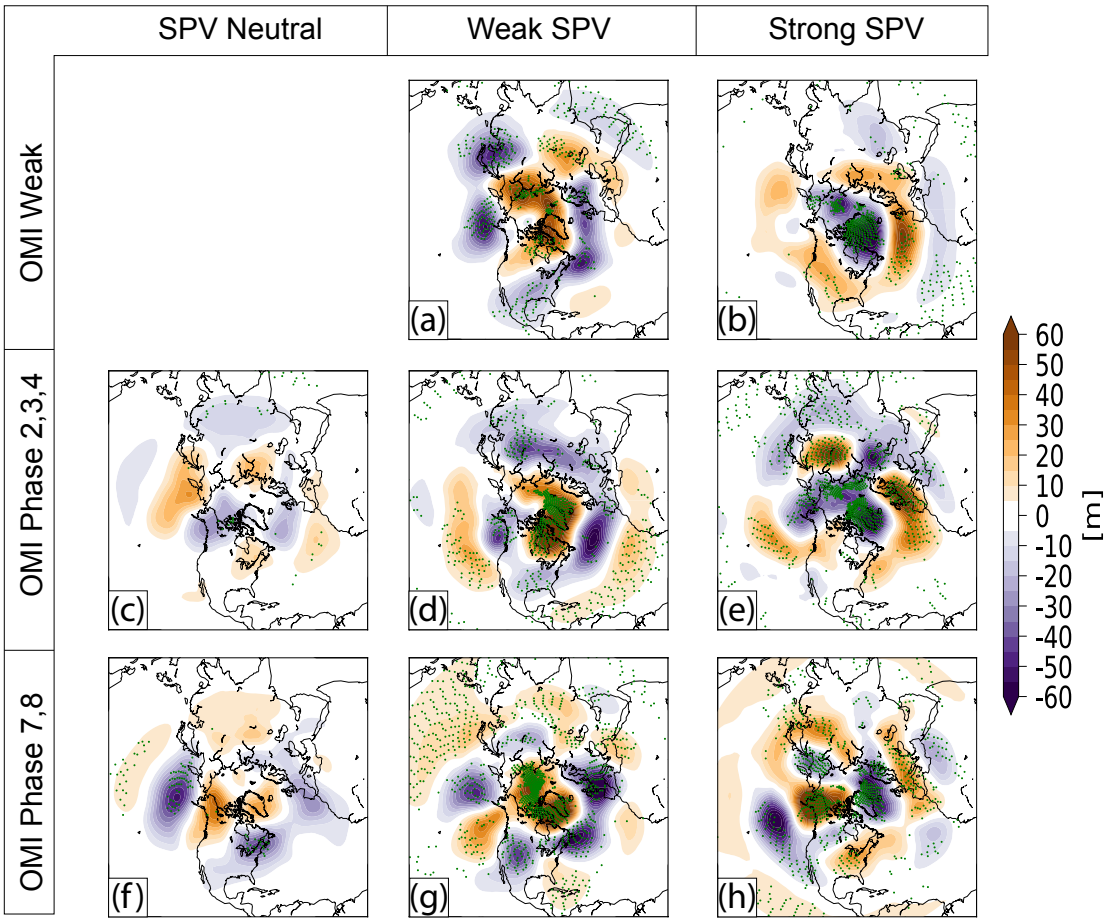

Figure 3.1: 500 hPa GPH anomaly composites (m) for +10 to +14 days after (a) Weak SPV + weak OMI, (b) Strong SPV + weak OMI, (c) OMI phases 2,3,4 + Neutral SPV, (d) OMI 2,3,4 + weak SPV, (e) OMI 2,3,4 + strong SPV, (f) OMI phases 7 & 8 + Neutral SPV, (g) OMI 7,8 + weak SPV, and (h) OMI 7,8 + strong SPV events. Green stippling represents 66% of composite members agree on the sign of the total composited anomaly. Composited for the months of October-March.

Next we examine the OMI + neutral SPV conditions to contrast with the SPV-only composites (Figs. 3.1c and 3.1f). During OMI phases 2,3,4 + neutral SPV (Fig. 3.1c) a wave

pattern emerges over eastern Asia and spans over northern North America, highlighted by a large positive anomaly over the North and Western Pacific and a strong negative anomaly over Alaska and northern Canada. While not very strong, a dipole pattern in the North Atlantic is prevalent in Fig. 3.1c. The 500 hPa GPH anomalies observed during OMI 7,8 + neutral SPV cases are almost opposite-signed to those in Fig. 3.1c. These GPHa patterns follow from previous literature (e.g Moore et al. 2010). This shows that although these pattern are during neutral SPV, they are still consistent with previous findings and are more associated with the OMI events alone.

The lack of significance in Figs. 3.1c,f indicates that these composite patterns have large variability spatially which may be resulting from a large sample size of multiple OMI phases. The most consistency within the OMI patterns can be observed during phases 7,8 over the North Pacific and the northeast North America (Fig. 3.1c). A few factors may be forcing these results such as, large spatial variability from event to event. Also, throughout the cold season, the MJO may interact with tropospheric weather patterns differently. Early season events (October through December) may produce different wave patterns than events that occur later in the active season (January through March). This is discussed further in next section.

Having verified our compositing technique works for the stand-alone cases, we now explore the combined MJO-SPV cases. Comparing Fig. 3.1d with Fig. 3.1c, the North Pacific pattern shows a statistically significant positive anomaly that is shifted eastward toward western North America, indicating that the inclusion of the OMI 2,3,4 + weak SPV offers more control over the pattern within this region. The joint influence composite also resembles the weak SPV + weak OMI pattern in the Arctic toward the Atlantic side. The joint OMI 2,3,4 + strong SPV (Fig. 3.1e) establishes a zonally oriented dipole of negative height anomalies to the west and positive height anomalies to the east within the North Pacific.

Next, we examine +10-14 days after joint SPV+OMI 7,8 events, and their contrast to independent SPV and MJO events. OMI 7,8 + weak SPV joint cases (Fig. 3.1g) maintain a negative height anomaly in the North Pacific, while it also constructively interferes strongly with the pattern of the weak SPV + weak OMI, over the Arctic and European regions. This can also be observed through the constructive interference of the negative anomaly annular pattern in the mid-latitudes and its significant pattern recurrence. While Fig. 3.1g display constructive interference of the joint influence patterns, Fig. 3.1h shows strong destructively interfered patterns. OMI 7,8 + strong SPV influences only the Atlantic and Europe regions to maintain the strong SPV pattern, seen in Fig. 3.1b. The annular pattern observed through the strong SPV is also destroyed, while the OMI 7,8 maintains a negative height anomaly pattern in the North Pacific. This destructive interference pattern is consistent throughout the events composited (Fig. 3.1h, green stippling).

3.1.1 Intraseasonal Changes of MJO Influence

Our analysis spans the entire cold season, however, changes to these patterns may occur throughout this period and may be lost to the relatively long seasonal composite. In surface temperature composites of MJO events that occurred over a selected three months, provided by the NOAA's Center for Weather and Climate Prediction Climate Prediction Center [1], it is shown that the MJO impacts weather patterns differently in the early active season compared to the late active season. In some extreme cases, regions can experience sign reversal of SAT anomaly patterns. To investigate these patterns of the MJO and SPV events, both individual and joint were separated into two different groups of months. The first group is for events that occur in the months of October through December, and the second group is in the months of January through March. All of the comparisons made here are in reference to Figure 3.1. Looking first at the MJO events, OMI 2,3,4 does not project a strong positive height anomaly in the North Pacific. This affects the patterns in this

[1] http://www.cpc.ncep.noaa.gov/products/precip/CWlink/MJO/Composites/Temperature/

region during the joint composite, which also lack this signature. OMI 2,3,4 and weak SPV are still destructively interfered, while OMI 2,3,4 and strong SPV are constructively interfered. Unlike OMI 2,3,4, OMI phases 7 & 8 produce a large negative anomaly in the North Pacific, consistent with the total composite (Figure 3.1f). In the joint composites, the anomalous pattern in the Pacific is shifted to the east. Consistent with previously discussed composites, OMI 7,8 and weak SPV produce constructive interference, and OMI 7,8 and strong SPV produce the strongest destructive interference.

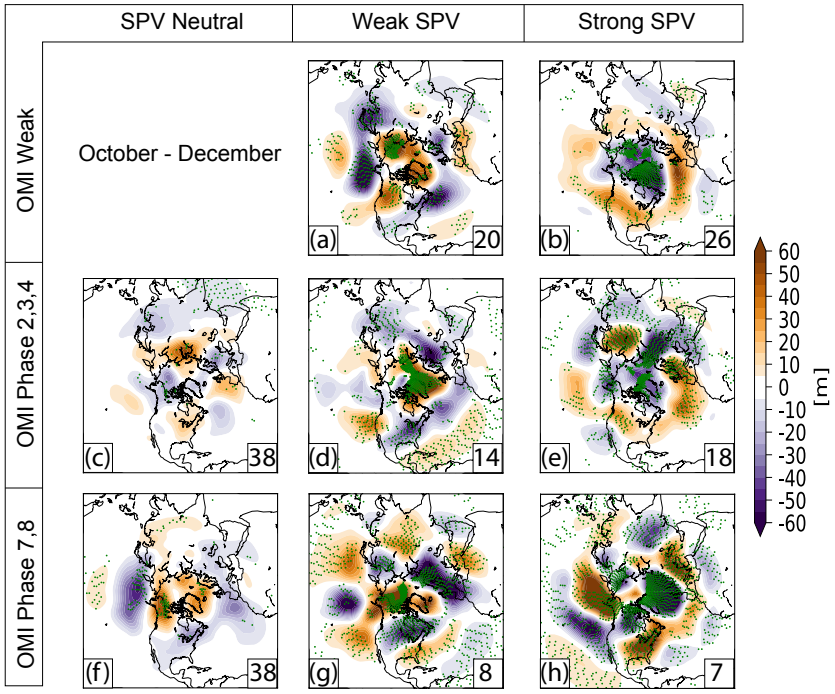

Figure 3.2: Same as Figure 3.1 except for months of October-December with event sample size (lower right corner).

MJO events that occur later in the active season, produce slightly different patterns than those earlier in the season. In Figure 3.3c, OMI 2,3,4 displays a positive height anomaly in the North Pacific, consistent with the full winter season composite. This then allows for the joint composites to retain a similar signal in this region, more closely replicating the full composite in Figure 3.1. OMI 7,8 (Figure 3.3f) projects similar effects onto the northern

hemisphere during these months as earlier in the season. Similar constructive and destructive interference is observed with the weak and strong SPV events, respectively. Although there are some slight changes in strength and positioning of the SPV composite, the same results are reached within the joint event composites. Similar relationships between the MJO and the SPV are formed during the two groups of composites as observed in the total composites. However, with few samples to work with initially, further categorization of composites makes it difficult to obtain robust results.

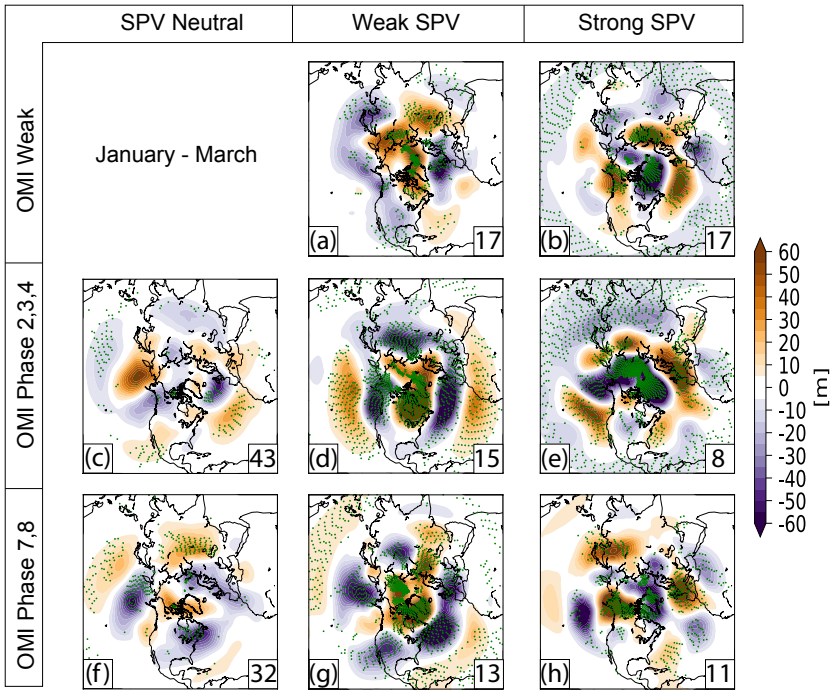

Figure 3.3: Same as Figure 3.1 except for months of January-March with event sample size (lower right corner).

3.2 250 hPa Zonal Wind Anomaly Composite Analysis

The jet stream can have strong effects on the weather patterns throughout the troposphere through its strength and position. As discussed in section 1.1, the state of the stratosphere directly impacts the speed and meridional extent of the tropospheric polar jet stream. Figure

3.4 shows the differences in jet stream structure (represented by 250 hPa zonal-mean zonal wind anomalies) for our different composite cases. Fig. 3.4a shows large areas of anomalously easterly zonal winds in the high latitudes for weak SPV + weak OMI events. The jet is shifted southward and is anomalously strong over the mid-latitudes. Large changes in the latitudinal placement of the zonal wind anomalies around the NH, is a result of a weak circulation in the stratosphere. Conversely, the strong SPV + weak OMI (Fig.3.4b) is represented by organized, confined westerly anomalies over the high latitudes. Through this contracted circulation, Arctic air is retained within the high latitudes, consistent with the observed negative temperature anomalies over the Arctic (see Fig 3.5b).

Transitioning not to neutral SPV cases, OMI 2,3,4, in Figure 3.4c, displays a region of anomalous westerly winds are observed over central Asia, north of the regions of enhanced convection for these phases (i.e. a retracted jet; Moore et al. 2010). These accelerated westerlies are forced by the strong height gradient, located between the jet and the enhanced convection. North of the suppressed convection (central Pacific), a region of anomalous easterly wind is observed, although the pattern is not significant. Zonal winds throughout the rest of the NH do not appear to be directly affected. Only a small area of significant westerly zonal wind is observed in the North Atlantic (Figure 3.4c).

Combined events of OMI 2,3,4 + weak SPV (Fig. 3.4d) again show destructive interference in the North Pacific. Here there is a split jet pattern over the western Pacific. Suppressed convection within the central Pacific is a possible cause behind this pattern, forcing the polar jet to keep a northward track across the Pacific. The retraction of the Asian-Pacific Jet over Asia is still forced by the regions of active convection. The weak SPV pattern maintains its southward extent over the eastern portions of North America, the Atlantic Ocean, and Europe. The combined events of OMI 2,3,4 + strong SPV produce a slightly modified version of the polar jet for this SPV phase. In Figure 3.4e, the westerly wind anomalies are still contained within the high latitudes in the region of the North Atlantic and Europe. However, over the North Pacific, the zonal wind anomalies are shifted

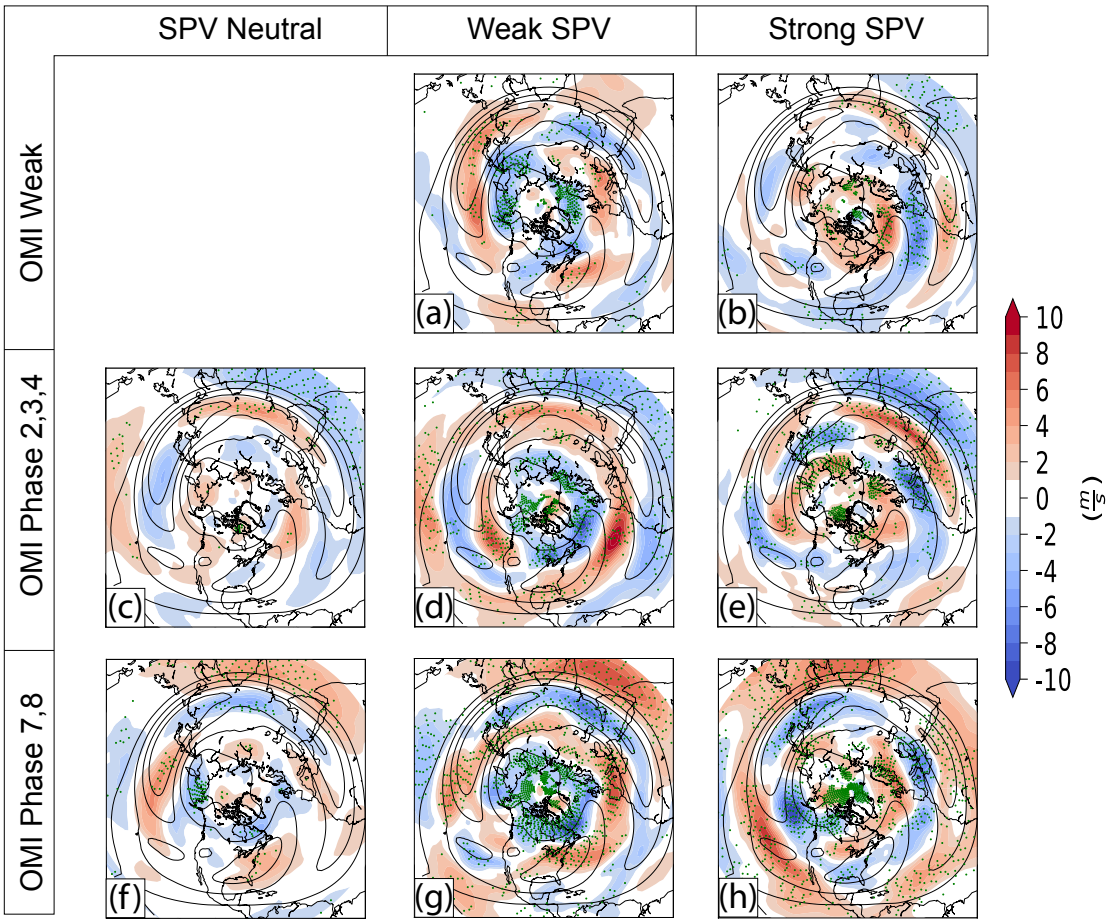

Figure 3.4: Same as Figure 3.1 except for 250 hPa zonal wind anomalies (ms^{-1}). Overlaid are contours of the climatological (1981-2010) zonal wind pattern. Westerlies (solid) and easterlies (dashed) are contoured from -40 to 40 on a 10 ms^{-1} interval, where zero line is omitted.

slightly southward, encouraging impacts more directly over the Pacific Northwest. Also, the retraction of the Asian-Pacific jet is shifted relatively far to the west, compared to that of the MJO-only pattern.

OMI 7,8 + neutral SPV (Figure 3.4f) exhibits a shift in the pattern of the Asian-Pacific Jet compared to OMI 2,3,4 + neutral SPV (Fig. 3.4c). Here the jet is accelerated over regions of the enhanced convection in the Pacific. Suppressed convection, now located within the Indian Ocean, causes easterly anomalies to be present over central Asia. Strong constructive interference is observed during the OMI 7,8, + weak SPV events (Fig. 3.4g). Here the southward positioning of the jet can be clearly observed in the mid-latitudes in an annular pattern, allowing the cold, Arctic air to impact lower latitudes. Consistent with the preceding analysis, this combined event exhibits the strong constructive interference compared to the remaining joint composites.

The combined event of OMI 7,8 + strong SPV (Fig. 3.4h) shows the strong destructive interference. The MJO continues to influence the pattern of the zonal wind within its region of the direct control, the central Pacific. However, the Arctic pattern for this event is almost completely unrecognizable. The tightly contracted jet observed in the SPV-only composite is not present within the combined event. Instead, the jet exhibits a southward shift over eastern North America, the Atlantic, and Europe. Within the North Pacific there is no resemblance of a strong SPV pattern, with easterly anomalies taking place in high latitudes. With a relatively weak SPV appearance, this combined event continues to exhibit the strongest destructive interference.

Using the zonal wind anomalies as a representation of the position and strength of the tropospheric jet streams, storm tracks and cold weather regimes may be influenced by the MJO and the SPV. Surface cyclones are impacted by the positioning of this jet and help to influence regions of anomalously cold air (Baldwin and Dunkerton 2001). Likewise, temperature anomalies and surface impacts are also influenced by the MJO-SPV relationship, which is explored in section 3.3.

The themes of pattern consistency among the different composite cases, observed in Figures 3.1, are emphasized within these composites as well. The areas of significance within the combined events increase compared to the individual counterparts. Using the two climate modes together to diagnose atmospheric patterns continues to provide increased information and consistency in the anomalous patterns produced.

3.3 Surface Air Temperature Anomaly Composite Analysis

While the 500 hPa GPHa and anomalous zonal wind composites give insight into the main circulation pattern, we next examine the SAT anomaly composites to highlight sensible weather impacts at the surface (Figure 3.5). The SAT anomaly composite for the SPV + weak OMI cases are displayed in Fig. 3.5a,b. Patterns observed here match those of previous studies (e.g., Thompson and Wallace 2000; Waugh et al. 2017), showing a warm (cold) Arctic for weak (strong) SPV + weak OMI. Similar to that of the 500 hPa composites (Fig. 3.1a,b), the significance pattern associated with the weak SPV + weak OMI (Fig. 3.1a) are less concentrated in the Arctic, located over northern North America and northern Asia. The strong SPV + weak OMI (Fig. 3.1b) is associated with more confined areas of significance over the Greenland. The changes in consistency among the SPV regimes could result from variability in the way the SPV weakens or is displaced from the Arctic.

We now analyze the response in surface temperature to MJO convection located in the Indian Ocean. OMI 2,3,4 + neutral SPV in Fig. 3.5c, shows a primarily cold Arctic with warm temperature anomalies positioned over much of North America, but little of the signal is statistically significant. When considering events of OMI 2,3,4 + weak SPV (Fig. 3.5d), we see constructive interference with the OMI 2,3,4 + neutral SPV (Fig. 3.5c) and weak SPV + weak OMI (Fig. 3.5a) patterns over the Arctic, but destructive interference over the northeast United States. For the OMI 2,3,4 + strong SPV cases (Fig. 3.5e), large significant areas of constructive interference appear across the NH.

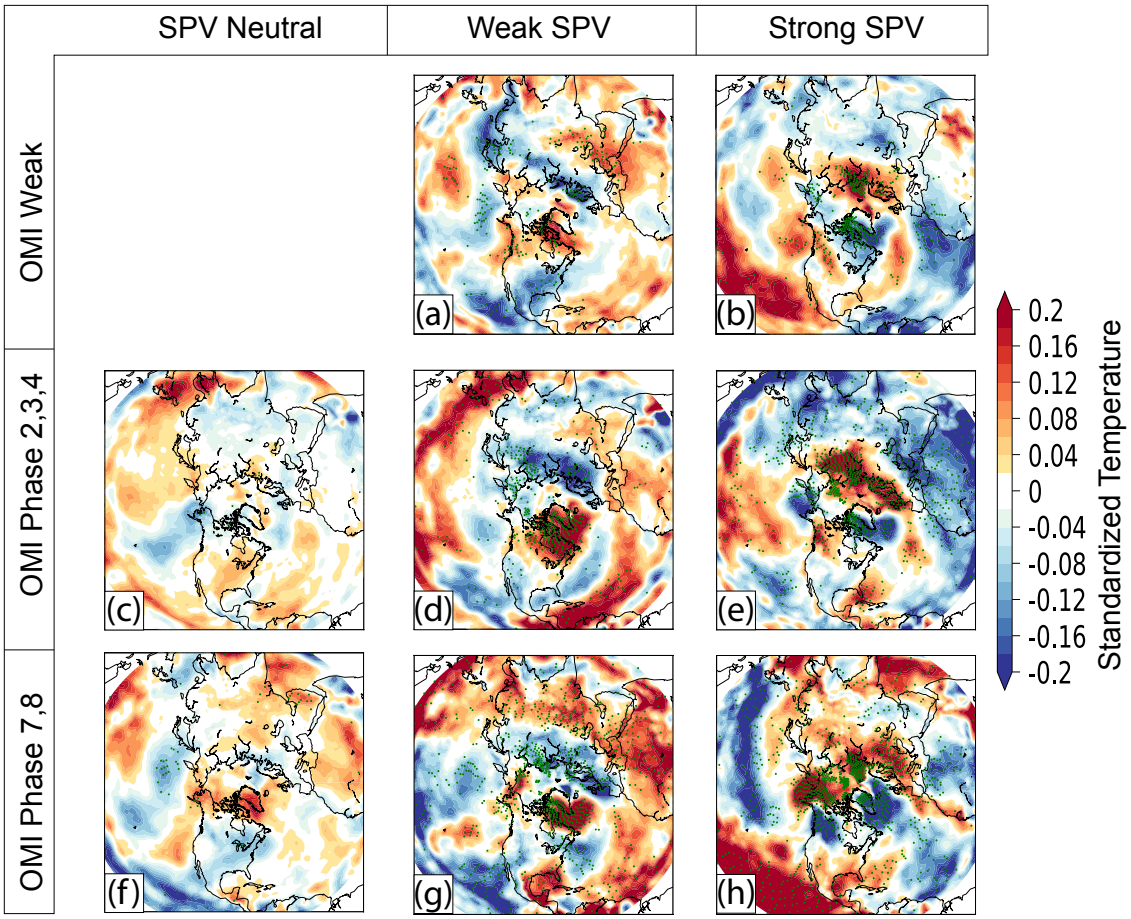

Figure 3.5: Same as Figure 3.1 except for standardized surface air temperature anomalies.

Figure 3.5f shows the pattern for OMI 7,8 + neutral SPV events. Here the OMI 7,8 + neutral SPV resembles the weak SPV + weak OMI, with negative anomalies in the mid-latitudes and broad positive anomalies over the Arctic. Significance over Greenland, the Northeast U.S., and the Western Pacific depict patterns that are relatively consistent for these regions during OMI 7,8. Events with both OMI 7,8 + weak SPV (Fig. 3.5g) show constructively interference (Fig. 3.5f, Fig. 3.5a). Events of OMI 7,8 + strong SPV in Fig. 3.5h, on the other hand, show the most destructively interfered pattern. This interference mainly takes place within the Pacific and on the Pacific side of the Arctic and North America. The destruction of a strong SPV + weak OMI Arctic pattern in these regions is likely due to the direct influence of the wave pattern generated by the MJO during phases 7 & 8.

Throughout the composites of 500 GPHa, 250 hPa zonal winds, and SATa, a few key features emerge. Through all combinations of the MJO and SPV, the SPV maintains control of the pattern over the North Atlantic and Europe. Also, the influence the MJO pattern is most evident over regions that are closest to the Pacific, where the wave pattern generated by the MJO most easily reaches without modification. As observed in the 500 hPa composites, through subjective analysis, the most constructive (destructive) interference seems to occur during the OMI 7,8 + weak SPV (OMI 7,8 + strong SPV), in comparison to the OMI 2,3,4 joint events. Finally, the patterns of the combined cases are relatively more consistent than their independent counterparts.

3.4 Blocking Frequencies

Another significant surface weather impact occurs in conjunction with atmospheric blocking episodes. Atmospheric blocking impacts extreme winter weather, such as cold air outbreaks, and storm pattern and frequency (Berggren et al. 1949; Austin 1980; Tyrlis and Hoskins 2008a,b). Associated with the anomalous GPH patterns (Fig. 3.1), atmospheric blocking should project the same patterns of interference seen throughout the analysis so far.

Figure 3.6 shows blocking frequency for a latitude band of 40.5^oN to 60^oN. This latitude band is of greatest interest due to the impact that blocks occurring in this region can have on regions of dense population. The weak and strong SPV + weak OMI patterns differ in the regions where they experience the largest deviations from climatology. In Fig. 3.6a, the weak SPV + weak OMI has a frequency over the Atlantic and Europe that is much less than the climatology, while Asia and the Western Pacific experience a relatively greater frequency of blocking regimes. High-latitude blocking is observed in the North Atlantic when analyzing the weak SPV + weak OMI composite of 500 hPa GPHa (Fig. 3.1a). However, analyzing the 40.5^oN to 60^oN latitude band, there is a large region of negative height anomalies in this region. The strong SPV + weak OMI events (Fig. 3.6b) do not exhibit the large deviations from climatology. These blocking composites represent regions of atmospheric GPH features that act to impact the mid-latitude sensible weather patterns through anomalously increasing meridional flow.

OMI 2,3,4 + neutral SPV (Fig. 3.6c) show a blocking frequency pattern that is very similar to climatology, with a small decrease east of the dateline. This decrease of frequency within this region is also experienced during the OMI 2,3,4 + weak SPV in Fig. 3.6d. As seen in Sections 3.1, 3.2, 3.3, destructive interference occurs in the Atlantic and Europe regions showing near climatological levels of blocking frequency. Blocking frequency for the OMI 2,3,4 + strong SPV events (Fig. 3.6e) show the western Atlantic sector as relatively low blocking frequency, while east of 0^o longitude the pattern is very similar to climatology. Over the western Atlantic, Fig. 3.6e displays a component of destructive interference through significantly negative blocking compared to climatology. This is not consistent with the composite analysis of OMI 2,3,4 + strong SPV. Through the 500 hPa GPHa, 250 hPa U-wind and SATa composites, this pattern case should be constructively interfered. However, it is important to note that the regions of greatest variability so far observed, one being North America, shows significant blocking patterns not seen in either OMI + neutral SPV or SPV + weak OMI.

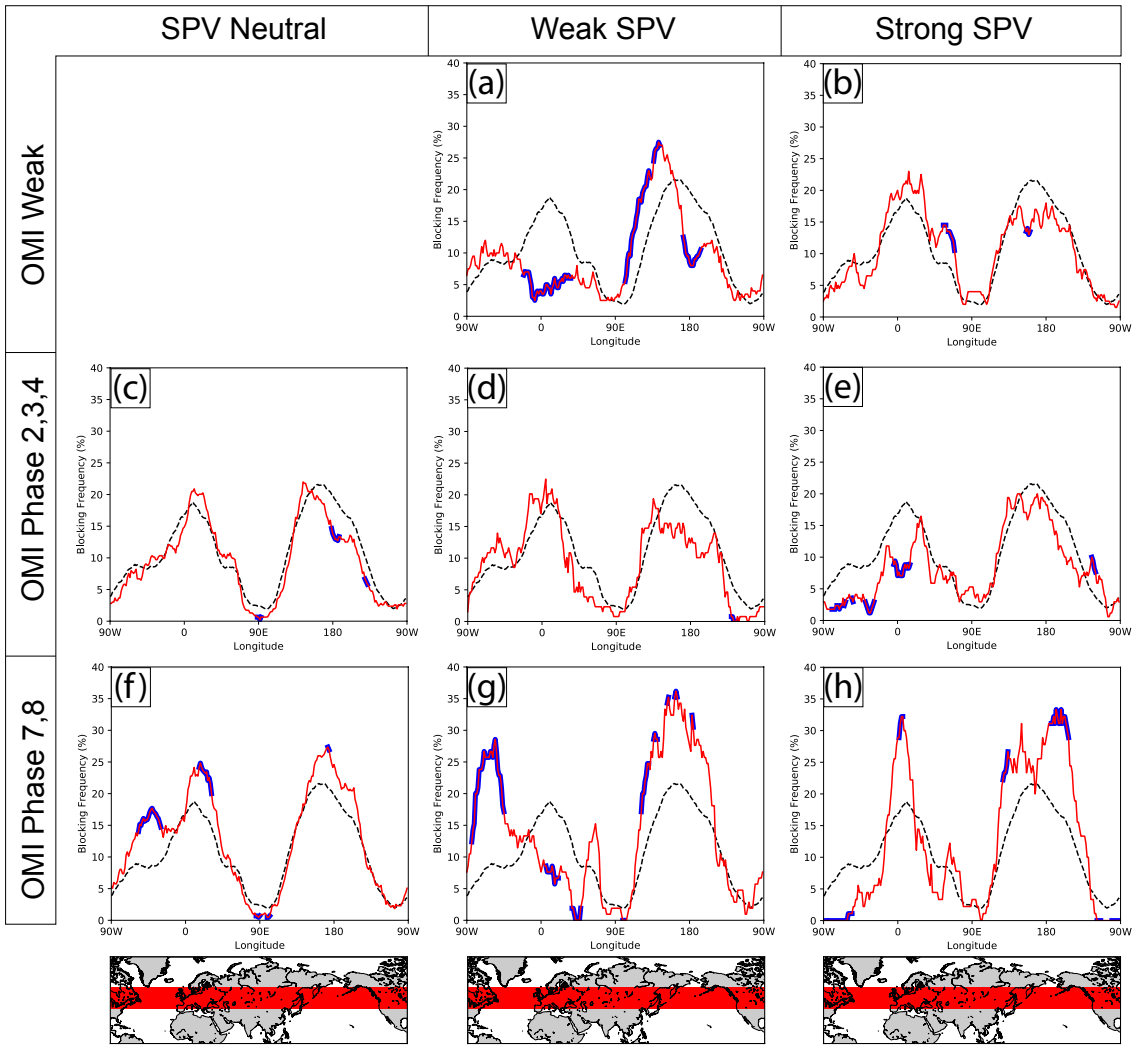

Figure 3.6: (solid red) Tibaldi and Molteni (1990) blocking index for latitudes 40.5^o – 60^oN, centered on 90^oE, shown for various MJO-SPV cases. (dashed black) Total October-March blocking climatology. Thick blue line denotes 90% significance found using Monte Carlo testing of 5000 interations. For reference, the region of blocking analysis (red swath) is overlaid on a map of the NH, matching the longitudinal orientation of the blocking composites.

Examining blocking frequencies for OMI 7,8 + neutral SPV cases (Fig. 3.6f), both the Atlantic/Europe and Pacific sectors experience a relative increase in blocking frequency. OMI 7,8 + weak SPV (Fig. 3.6g) shows constructive interference, consistent with previous observations of 500 GPHa and SATa. OMI 7,8 + strong SPV, in Fig. 3.6h, show themes of destructive interference in the Atlantic. Although there is a large spike in blocking frequency at 0^o longitude, the remaining regions surrounding the Atlantic have relatively less blocking frequency compared to the strong SPV + weak OMI (Fig. 3.6b). The Pacific sector continues to show evidence that the MJO maintains strong control of the patterns in this region with large positive deviations in frequency from climatology.

Chapter 4

Analysis of Wave Propagation and Impacts

Through the results analyzed so far, both the MJO and the SPV influence particular patterns, together and separate of one another. However, as seen in the combined composite, there are cases of constructive and destructive interference of the large-scale weather patterns. These influences work through the changes in wave patterns and propagation that result interaction between the MJO or the stratosphere. As was discussed in Chapter 1, the MJO initiates Rossby waves that propagate poleward from the enhanced convection and into the mid- and high-latitudes (Frederiksen and Lin 2013). Wang et al. (2018) show that different locations of MJO enhanced convection change the stratosphere-troposphere interactions through influencing vertically propagating waves. The SPV is also responsible for changing the circumpolar wave pattern through change the speed of the stratospheric circulation (Baldwin and Dunkerton 2001; Kidston et al. 2015). Analyzing the dynamical wave propagation changes should offer more information into the dynamical interactions between the MJO and the SPV.

4.1 500 hPa Anomalous Eddy Geopotential Height Anomalies

To this point only tropospheric variables and diagnostic tools have been used to understand the relationship of the MJO and the SPV. Our next objective is to analyze how the stratosphere-troposphere interactions lead to observed changes in the circulation associated with the MJO and SPV. First, we analyze the wave patterns at the top of the troposphere, where waves have the greatest potential to propagate into the stratosphere. 250 hPa anomalous eddy heights (Z'^{*}) are found first by removing the zonally averaged GPH ($[Z]$) from the full GPH field (Z), then by removing the time 1981-2010 averaged eddy heights ($\overline{Z^{*}}$)

from the full eddy geopotential heights (Z^*) (shown in Equation 4.1 & 4.2) (Delworth and Coauthors 2006).

$$Z^* = Z - [Z] \tag{4.1}$$

$$Z'^* = Z^* - \overline{Z^*} \tag{4.2}$$

These values are then composited, with the methodology discussed in Section 2.2. By using 250 hPa Z'^* and analyzing the changes in the positioning of these waves with respect to climatology, we may gain a better understanding of the positioning of persistent waves near the tropopause. This diagnostic will also give an indication of the way in which the troposphere-stratosphere interactions are reflected onto the wave patterns in the upper troposphere.

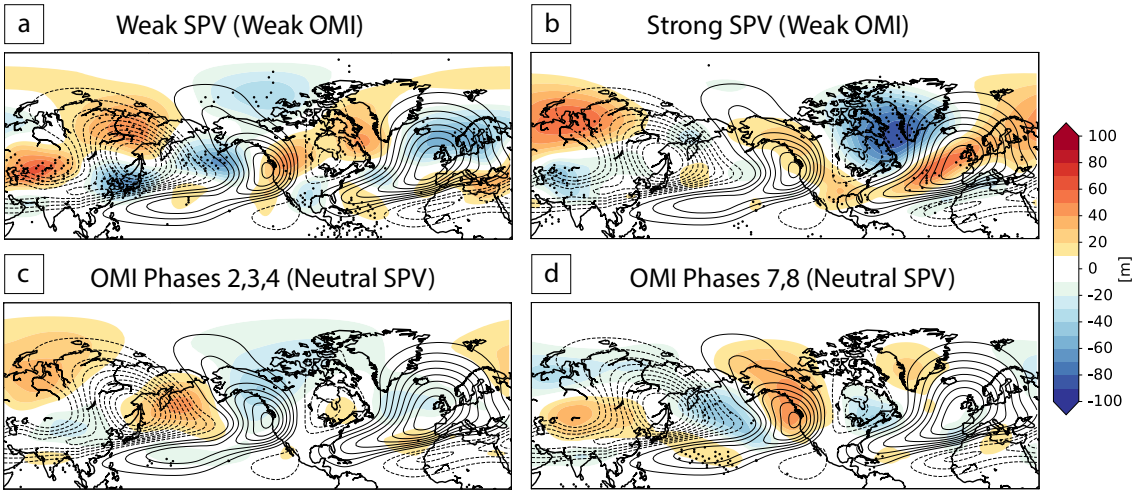

Figure 4.1: 250 hPa anomalous eddy geopotential heights +10 to +14 days after event (shading; m) and mean event composites are compared to the October-March climatological 250 hPa eddy geopotential heights (black contours; m) for (a) weak SPV + weak OMI), (b) strong SPV + weak OMI), (c) OMI 2,3,4 + Neutral SPV, (d) OMI 7,8 + neutral SPV. Solid (dashed) lines represent positive (negative) values; zero contour is omitted. Significance (black stippling) represents locations where 66% of composite members agree on sign of composite.

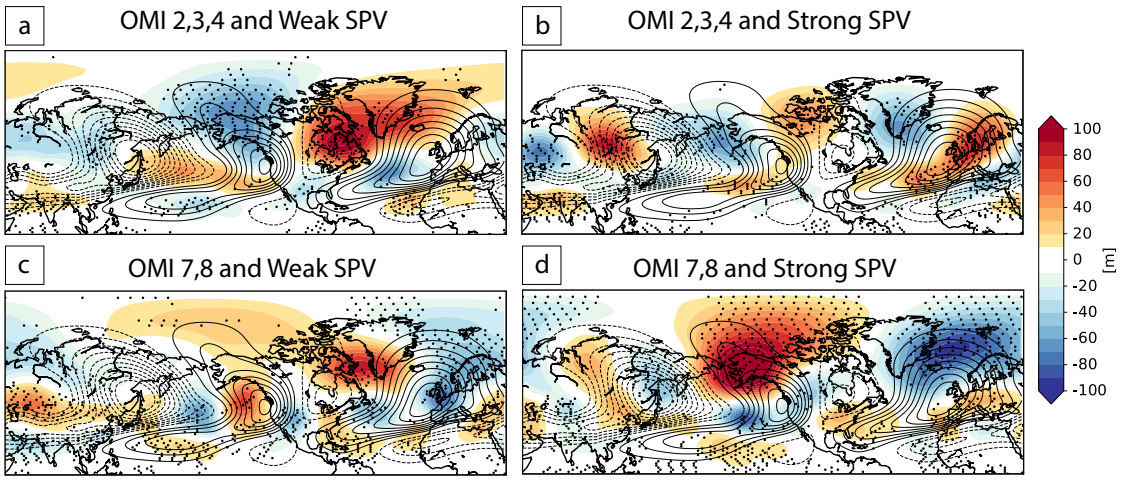

Figure 4.2: Same as Figure 4.1, but for (a) OMI 2,3,4 + weak SPV, (b) OMI 2,3,4 + strong SPV, (c) OMI 7,8 + weak SPV, and (d) OMI 7,8 + strong SPV events.

When observing the 250 hPa eddy GPH for +10-14 days after the SPV, there are two separate regions of focus for the two phases of the SPV. In Figure 4.1a, the weak SPV + weak OMI shows large regions of low eddy heights in the North Pacific. These negative eddy heights extend east from a large, significant region of negative eddy heights located over eastern Asia. This is joined by positive eddy heights along the west coast of the North America, which is small in comparison to climatology. This feature is consistent between the weak and strong SPV + weak OMI phases. However, the main focus for strong SPV + weak OMI (Fig. 4.1b) is the more amplified pattern in the North Atlantic and northeast North America. Here the strong SPV + weak OMI is associated with negative eddy anomalies over the western North Atlantic, which is shifted eastward from climatology. Positive eddy heights extend across much of the Atlantic to northern Europe. The pattern in the North Atlantic for the strong SPV + weak OMI is much stronger in comparison to that of the weak SPV + weak OMI. The weak SPV + weak OMI (Fig. 4.1a) shows to weaken the climatological pattern of the eddy heights of negative anomalies over northeast North America, while broadening the positive anomalous eddy pattern in the Central Atlantic.

The position of the enhanced convection of the MJO shows to also have a relationship with the change in the areas of strongest anomalous eddy GPH. This was first seen in the wave patterns in the 500 hPa GPHa in Fig. 3.1. Enhanced convection located in the Indian Ocean in Fig. 4.1c (OMI 2,3,4), favors negative eddy anomalies over eastern Asia. Many regions during this event display an anomalous pattern that is opposite of the climatological pattern. In its entirety, the OMI 2,3,4 + neutral SPV shows increased variability of the position and strength of the eddy height pattern, specifically in the North Pacific, weakly consistent with the position of these waves from climatology. Enhanced convection in the western-central Pacific Ocean (OMI 7,8 + neutral SPV) displays a different relationship with the anomalous wave pattern compared to when the convection is located in Indian Ocean (Fig 4.1d). OMI phases 7 and 8 show to produce an enhanced negative eddy anomalies over the north-central Pacific. An amplified pattern across North America can also be observed during OMI 7,8 + neutral SPV that was not observed during OMI 2,3,4 + neutral SPV. Overall, OMI 7,8 + neutral SPV act to amplify the climatological pattern, with the main focus placed on the North Pacific.

Figure 4.2 presents the 250 hPa anomalous eddy geopotential height composites for the conditional MJO/SPV cases. Observing OMI 2,3,4 + weak SPV (Fig. 4.2a) an amplified pattern of anomalous eddy heights downstream of enhanced convection strengthens with respect to OMI 2,3,4 + neutral SPV. By contrast, the large region of negative eddy height anomalies in northeast Asia extend into the Arctic, shifting the positive anomaly throughout the Pacific to the south. A large region of positive eddy height anomalies extends from North-Central North America to the North Atlantic. The OMI 2,3,4 + strong SPV event (Figure 4.2b) encourages a replica of the strong SPV + weak OMI pattern, but with the anomalous pattern shifted to the north. A clear anomalous wave pattern, originating over Eastern Asia, can be traced eastward across the Northern Hemisphere. During this combined OMI 2,3,4 + strong SPV event, there is strengthen constructive interference in the stationary wave pattern, produced by the strong SPV + weak OMI.

Combining the OMI 7 and 8 phases with the SPV phases also acts to modify the wave pattern. Figure 4.2c shows constructive interference of the weak SPV eddy anomaly pattern, specifically over North America and the North Atlantic. Compared to the patterns in Fig. 4.1d, the pattern across North America encourages the colder temperature patterns that are observed in Fig. 3.5. The anomalous wave patterns in the North Atlantic are not organized, as in the weak SPV + weak OMI composite. Here, the wave pattern, like in Fig. 4.1a, deviate from the climatological pattern. OMI 7,8 + strong SPV events (Fig. 4.2d) maintain the pattern of the OMI relationship in the Pacific, with anomalies shifted poleward from climatology. Also, anomalously positive eddy heights located over Alaska are a consistent relationship produced by these events. A decrease in the magnitude of the wave pattern in the North Atlantic can be observed during these combined events, showing destructive interference of the OMI onto the strong SPV patterns.

Here, we observe changes in the anomalous eddy geopotential height patterns, with respect to the climatological pattern, connected to the MJO-SPV relationship. Also, through the composites of the joint OMI-SPV events, high-latitude anomalous eddy heights are amplified, with greater recurrence of anomalous patterns throughout the events. Compositing the OMI and the SPV together provide different patterns that are not observed during the individual events. Some of the features observed within the blocking analysis are observed in these eddy height composites. So far, we have observed that the OMI-SPV joint composites have changed large scale flow patterns, as well as, sensible impact patterns, but all these have been observed in the troposphere. How do the changes in these wave patterns, specifically in the high-latitudes of the upper troposphere, act to influence the stratosphere-troposphere relationship?

4.2 Dynamical Analysis of Stratosphere-Troposphere Interactions

So far, the analysis has focused on the tropospheric impacts of the relationship between the MJO and the SPV. In this section, we examine whether vertically propagating Rossby

waves, associated with the different composite cases influence changes in stratosphere-troposphere interactions. Combining events have so far displayed that large scale patterns are influenced by the MJO-SPV relationship. Zonal mean zonal wind tendency represents how the speed of the zonal mean zonal wind changes with time +10-14 days after the OMI-SPV cases (Figure 4.3). Here, large deviations of the tendency patterns are observed when comparing the combined events to the independent OMI and SPV events. Observed changes throughout the troposphere and stratosphere are investigated through the use of EP-Flux and its divergence (Figure 4.4). The EP-fluxes and their respective divergence and convergence are plotted for all of the categorized OMI and SPV cases +10-14 days after event start. Figures 4.4a,b agree strongly with the results discussed in Thompson et al. (2006). The weak (strong) SPV + weak OMI (Fig. 4.4a(b)) shows relatively strong (weak) downward EP-flux, representing anomalous downward wave propagation. There is a large spatial coverage of convergence within the troposphere as well, that will lead to the deceleration of the tropospheric polar vortex. The troposphere also contains more regions of divergence, acting to accelerate westerly motion. Here the divergence in the stratosphere (Fig. 4.4b) does not directly correspond with large regions of acceleration of the zonal mean zonal wind (Fig. 4.3b).

Both the EP-flux vectors and divergence are weaker in magnitude in the OMI 2,3,4 + neutral SPV than either OMI weak case (cf. Fig. 4.4c, Figs. 4.4a,b). There is no significant EP-flux relationship with OMI 2,3,4 + neutral SPV in the stratosphere (Fig. 4.4c). When analyzing the combined events of the OMI 2,3,4 + weak SPV (Fig. 4.4d), convergence is observed in the stratosphere, but not due to waves propagating upward from the stratosphere. Here, originating in the tropical troposphere propagate northward with no influence on the stratosphere. Similar to the weak SPV + weak OMI, waves in the troposphere propagate anomalously downward approximately north of 40^{o}N. With very little EP-flux convergence in the troposphere, this will promote a deceleration of the tropospheric polar vortex. The fact that there is a lack of any waves propagating vertically, means the OMI

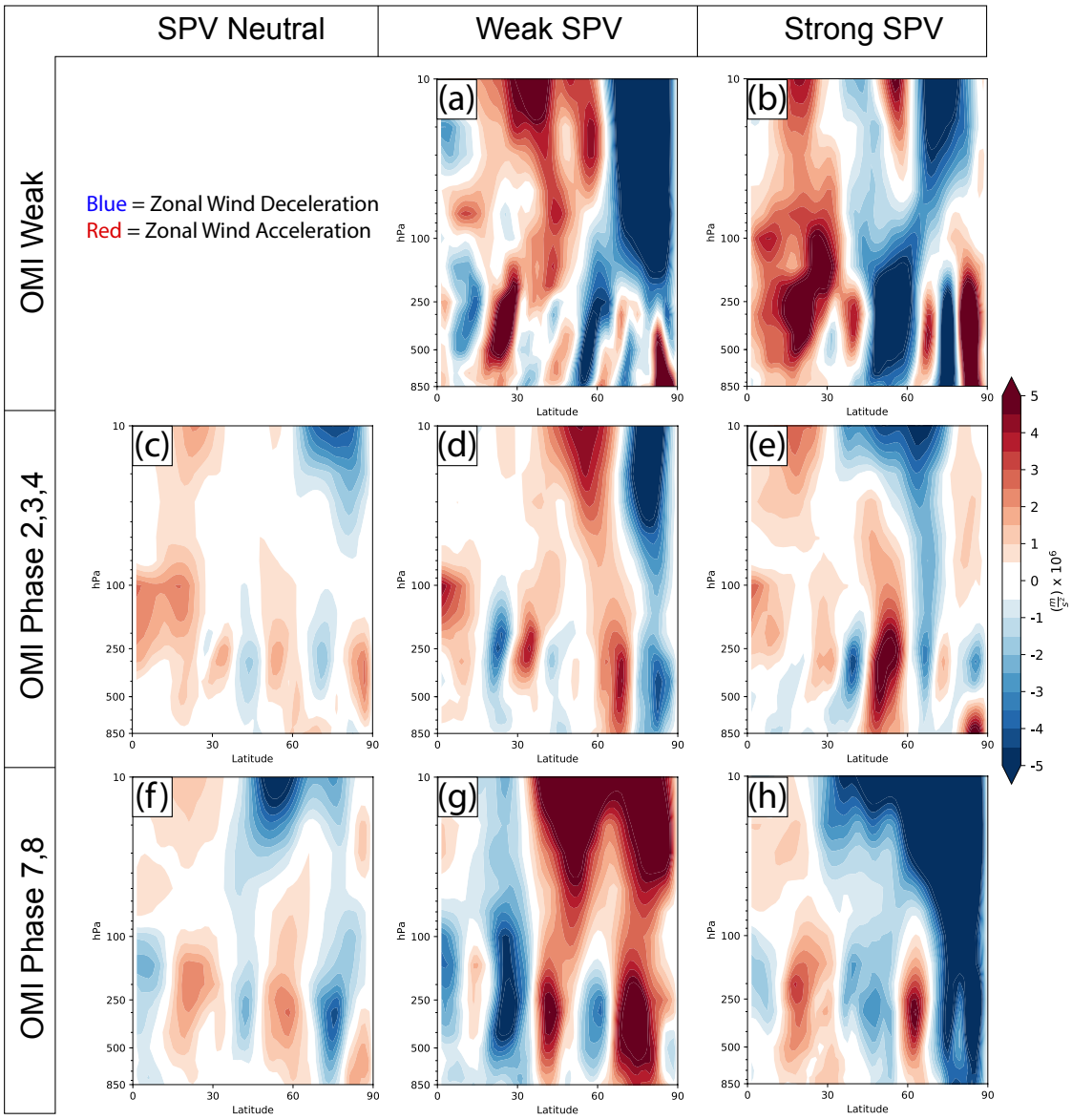

Figure 4.3: Zonal mean zonal wind tendency ($\frac{\partial \bar{u}}{\partial t}$) for various MJO-SPV events. Positive tendency (blue shading) and negative tendency are plotted from -5 to 5 ms^{-2}, with an interval of 0.5.

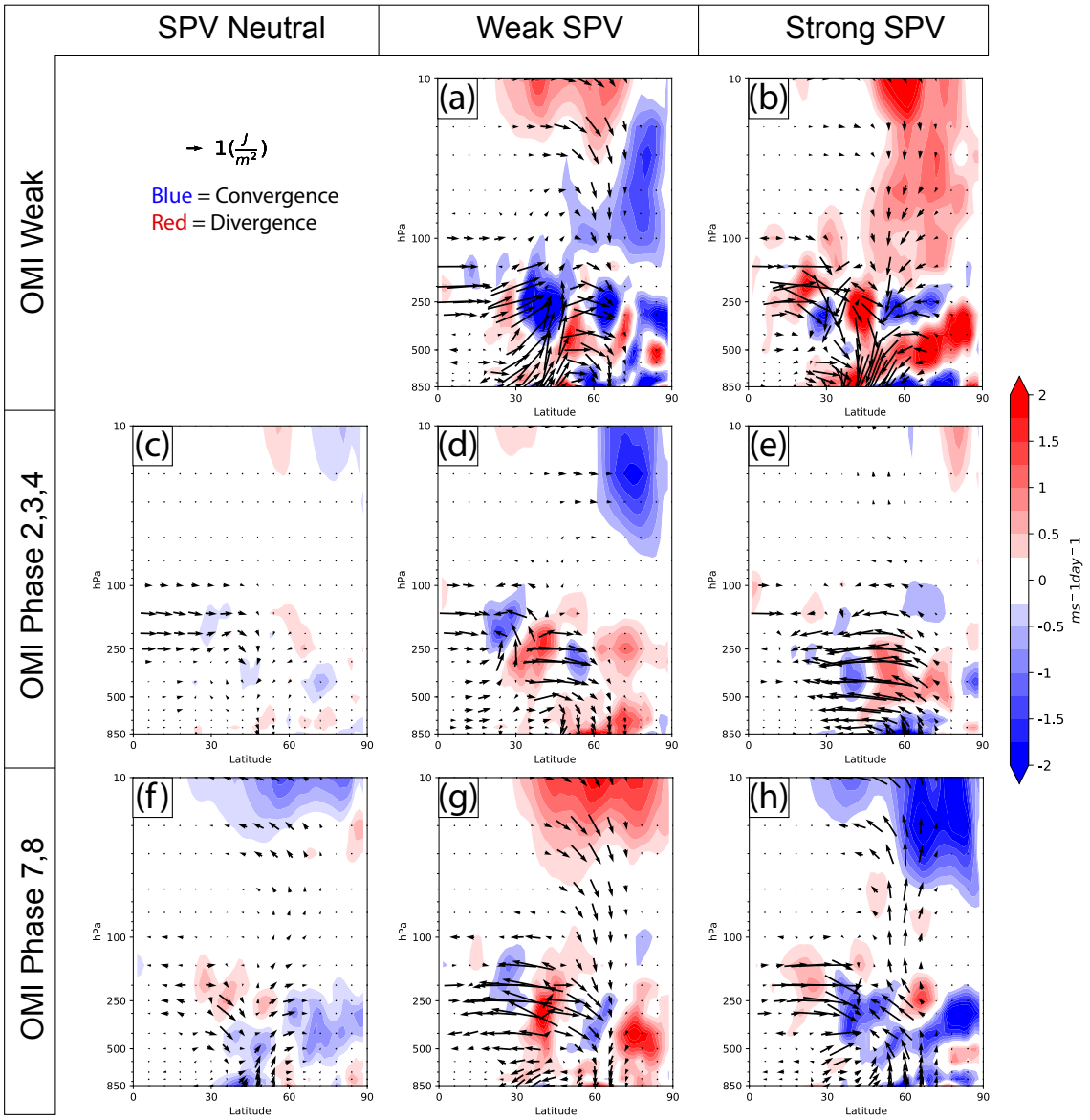

Figure 4.4: Scaled Eliassen-Palm flux (vectors, Jm^{-2}) and flux divergence (shading, $ms^{-1}\,day^{-1}$) for various MJO-SPV cases. EP-flux vector of magnitude 1.0 Jm^{-2} is used as reference. EP-flux divergence (red shading) and convergence (blue shading) is contoured from -2 to 2, with an interval of 0.25.

2,3,4 + weak SPV combined case displays destructive interference (Fig. 4.4a). The OMI 2,3,4 + strong SPV, in Fig. 4.4e, contains patterns seen in both the strong SPV + weak OMI and the OMI 2,3,4 + neutral SPV cases. With very little influence on the stratosphere by the MJO, the already existent strong SPV pattern will not be impacted by the waves contained within the stratosphere. In the troposphere, areas of divergence, similar to the strong SPV pattern, encourage an acceleration and anomalous poleward shift of the tropospheric polar jet stream.

Within these plots of OMI 2,3,4 + neutral SPV, as well as the combined events of the SPV, signals of waves propagating in or out of the stratosphere are nonexistent. Therefore, this analysis suggests that anomalous waves associated with OMI 2,3,4 are more confined to the troposphere with little to no influence on the stratosphere. Wang et al. (2018) finds that anomalous downward propagation of EP-flux occurs during years that have a relatively high occurrence frequency of MJO phase 4 events. Our results show the lack of a strong signal of anomalous wave propagation in or out of the stratosphere. Compared the weak OMI composite of the zonal mean zonal wind tendency, the OMI 2,3,4 combined events also do not exhibit as strong of a relationship with the zonal wind tendency in the stratosphere.

During Phases 7 and 8 of the OMI + neutral SPV, in Fig. 4.4f, upward propagation of waves into the stratosphere converge in the stratosphere. There is also convergence in the troposphere north of 60^oN. These two regions of convergence encourage a deceleration of westerlies. When combining these OMI + weak SPV events (Fig. 4.4g), similar patterns to that of the weak SPV + weak OMI are visible, with a large region of downward EP-flux and divergence in the stratosphere. Unlike the weak SPV + weak OMI, the combined case (Fig. 4.4g) does not display large regions of convergence in the troposphere, with only a small region around 60^oN present. This dynamical influence can be directly observed in the tropospheric wind pattern (Fig. 4.3g). Based on the pattern in the stratosphere, there is constructive interference with the weak SPV in this combined case of the OMI 7,8 + weak

SPV. The patterns of the OMI 7,8 + strong SPV (Fig. 4.4h) are primarily opposite to those observed in Fig. 4.4b. With an existent strong SPV during OMI 7,8, this pattern would lead to the breakdown and weakening of the SPV, as there is strong upward propagation of Rossby waves into the stratosphere and a large area of convergence coinciding (e.g. Garfinkel et al. 2012, 2014; Schwartz and Garfinkel 2017). Fig. 4.4g,h are further evidence that during OMI phases 7,8, there is constructive interference and destructive interference with the weak and strong SPV patterns, respectively.

Through dynamical analysis of the MJO-SPV relationship, patterns of constructive and destructive interference are continually revealed. OMI 2,3,4 and its joint relationship with the SPV shows to keep anomalous wave propagation within the troposphere. Although interacting with the tropospheric polar jet stream, influence on the stratosphere is not evident within analysis of the EP-fluxes and divergence. OMI 7,8, on the other hand, shows anomalous propagation of waves into and out of the stratosphere. The associated anomalous divergence shows relatively strong potential to influence the stratosphere.

4.3 Stratosphere-Troposphere Response to MJO Events

Within this section the OMI + neutral SPV interactions with wave dynamics and stratosphere - troposphere diagnostics are analyzed to understand the extent of the MJO's influence on the NH winter weather patterns. For this research it is important to address if the MJO and the SPV are two separate climate modes, working independently from one another, or if they are in fact influenced by the other. This would determine if the composite that have been analyzed thus far have been influenced by both of the modes or if they are an artifact of only one mode just working through the other. The two OMI event composites EP-flux displayed difference relationship with anomalous wave propagation into the stratosphere (Fig 4.4c,f). Phases 7,8 (Fig 4.4f) displayed EP-flux with a stronger signal compared to that of OMI 2,3,4. This raises a question of how the OMI + neutral SPV interact with the stratosphere to influence its state. Does the MJO influence patterns by first

influencing stratosphere-troposphere interactions, or does it only influence winter weather patterns through processes strictly in the troposphere?

We first analyze how the NAM index through the troposphere and the stratosphere changes around OMI + neutral SPV events. Anomalous zonal mean zonal wind is also analyzed, averaged between $60^o - 80^o$N, to determine the dynamical responses surrounding the start of the OMI event. OMI phases 2,3,4 have an associated trend toward a positive NAM pattern, where the zonal circulation strengthens throughout the atmosphere at approximately 15-20 days after the start of the MJO. This strengthening of the NAM index is associated with positive zonal wind anomaly. Prior to the OMI 2,3,4 event, the positive zonal wind anomalies are observed approximately 15-10 days before the event, this is reflected in the positive NAM index in the stratosphere at this time.

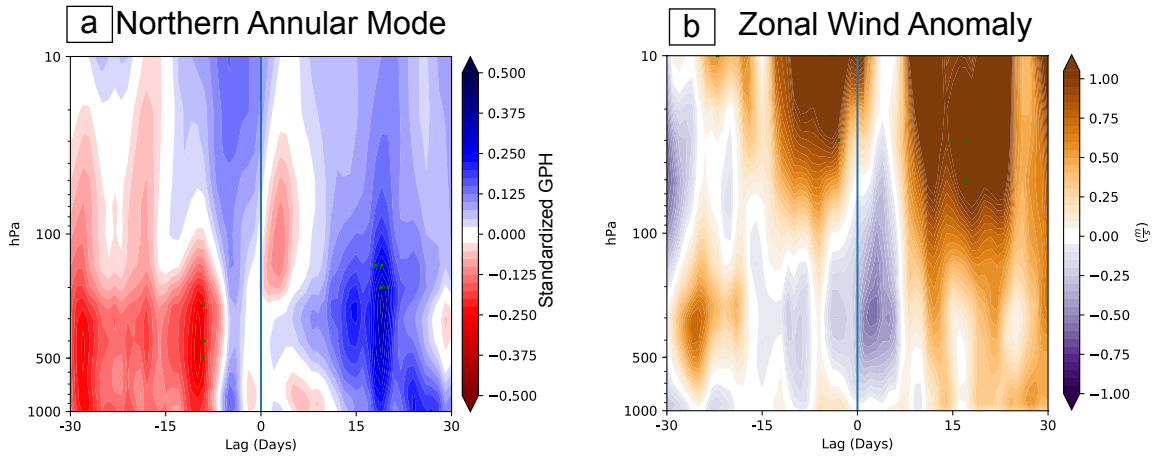

Figure 4.5: Pressure-time composites of the (a) GPH regressed onto the NAM index and (b) Zonal Mean Zonal Wind Anomalies (averaged over 60^oN to 80^oN) for OMI phases 2,3,4 + neutral SPV. Positive NAM values are contoured in blue and negative NAM is contoured in red. Day zero represents the start date of the OMI event (blue vertical line). Green stippling represents where 66% of the composite members agree on the sign of the (a) NAM index and (b) divergence shown in the composite mean.

Note that the positive NAM signal appears to initiate in the upper troposphere at about day 5, then strengthens simultaneously through the troposphere and stratosphere at day 10.

The 66% significance, however, is not observed until day 20, where the strongest positive NAM pattern is produced throughout the troposphere and stratosphere. This significance is rather small and is confined approximately the region of the tropopause. Unlike what is observed in Figure 1.2, the stratospheric signal does not initiate first with downward propagation following. Instead it appears that the MJO is associated with a change the NAM signal in the stratosphere and the troposphere at the same time. Referencing Fig. 4.4c, although OMI 2,3,4 + neutral SPV events shows very little affect on the stratosphere, the lack of upward wave propagation likely allows the stratosphere to maintain westerly circulation and accelerates 15-20 days after this event.

OMI phases 7 & 8 + neutral SPV shows a slightly different result of the effects that these phases has on the atmosphere. In Figure 4.4f, this group of MJO phases produced a pattern of upward propagating waves into the stratosphere with associated EP-flux convergence in the upper stratosphere. Differing from the effects of the OMI 2,3,4, phases 7 & 8 (Figure 4.6a) shows a NAM decrease and minimum in the troposphere at 5-10 days after the OMI event start date. Here the composite is significant, with composite members agree on the sign of the NAM index 66% of the time. The stratospheric NAM index indicates that it weakens after the troposphere weakens, similar to the pattern in Fig. 4.5a. The OMI 7,8 here is first influencing an anomalously weakened tropospheric circulation, only after that does this process propagate upward into the stratosphere. The minimum of the stratospheric NAM occurs at days 20-25 after the start of the OMI 7 & 8 event, where an associated anomalously weak stratospheric circulation takes place.

These composites are consistent with one another in their impacts onto the NAM pattern in the atmosphere. They first produce a NAM signal in the troposphere that then appears to propagate into the stratosphere. These events are not consistent with the plots in Figure 1.2, where the NAM pattern is initiated in the stratosphere and then propagates downward to impact the troposphere. These time-height plots also do not produce SPV events that last for the 30-60 days after the start day. Unlike the SPV + weak OMI events, the OMI +

neutral SPV initiated NAM patterns are short lived. For our analysis window of Pentad 2 (+10-14 days after event) the MJO's influence is still most strong within the troposphere. This means that the analysis discussed thus far (plotted for +10-14 days after event start) has been influenced by both the MJO and the SPV, and not solely the MJO influencing the stratosphere. This result is important for understanding how the MJO and the SPV relationship influences the patterns that we observe. In the analysis window of the results presented in this study, the OMI pattern does not influence the stratospheric pattern before impacting the observed tropospheric patterns. For this study, we can conclude that the relationships formed in the analysis are from both the SPV and the MJO, influencing the atmospheric pattern independently. However, without further analysis of the MJO's influence of the stratosphere-troposphere interactions, the question of how this process influences patterns on a longer S2S time scale (20+ days) still remains.

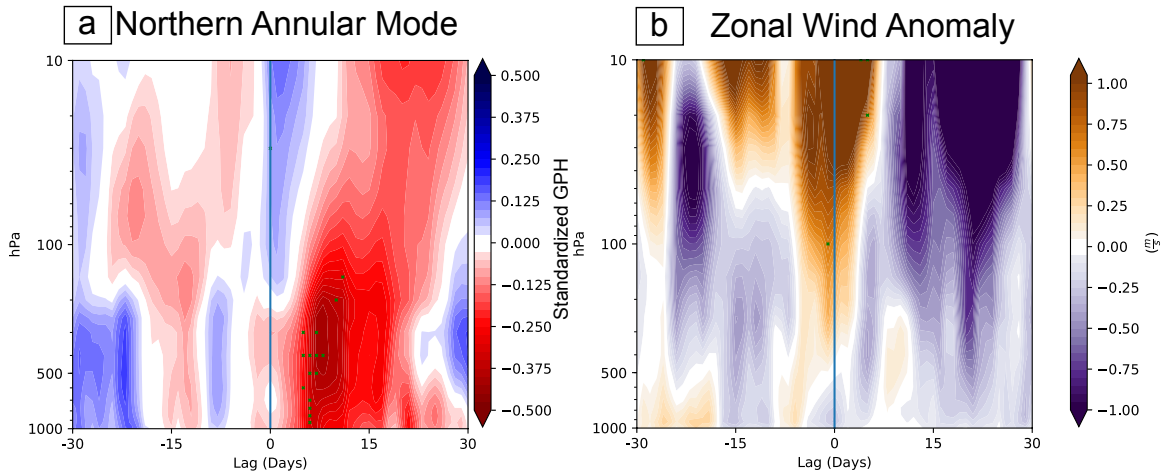

Figure 4.6: As in Figure 4.5, but for OMI phases 7 & 8 + neutral SPV.

Chapter 5

Discussion and Future Work

5.1 Discussion

This study presents analysis of the joint influence of the MJO and the SPV on the NH winter weather patterns. Major findings of the this research are as follows:

- The OMI maintains a relationship with the patterns in the North Pacific, while the SPV has a relationship with patterns over the North Atlantic and over Europe (Figs.3.1, 3.4, 3.5).

Through composite analysis these patterns of the independent OMI + SPV events were compared to their joint events. Here it was observed that the OMI maintains strong association with the patterns in the North Pacific. A north-south oriented dipole GPHa pattern, produced during OMI + neutral SPV composites, is recreated in the joint composites. Likewise, when analyzed individually, the SPV controls the pattern over the North Atlantic, Europe and the Arctic consistently throughout the composited events. When combined with the OMI, the North Atlantic and European regions remain consistent with the SPV + weak OMI composite. Little change is observed for these regions when combining the MJO and the SPV.

- Constructive interference in the patterns occurs during OMI 2,3,4 + strong SPV, and OMI 7,8 + weak SPV. Destructive interference occurs during joint events of OMI 2,3,4 + weak SPV, and OMI 7,8 + strong SPV. The composite of OMI 7,8 + strong SPV produces the strongest destructive interference relative to the two independent composites (Figs.3.1, 3.4, 3.5).

The patterns within the Arctic, although consistent throughout the SPV + weak OMI composites, have contribution from the OMI as well. The contribution to the pattern from

both modes was addressed throughout this study as interference of the SPV + weak OMI pattern. Constructive interference occurred when the SPV + weak OMI pattern appeared to be strengthened by the particular joint event, while destructive interference occurred when the SPV + weak OMI pattern was not like that of the joint event projection. These cases of interference are examples of information that is gained through using the joint events. Here, predictability of these events, using either the MJO or the SPV separately would not properly account for the interaction between the two modes. The destructive patterns show large regions (North America and Asia) where, if forecast for, would produce the wrong sign anomaly using either event separately. This evidence displays that predictability for joint events of the OMI + SPV would greatly increase if using both modes together as forecast tools. Separately, they do not properly handle the joint events, specifically during events that act to destructively interfere. This directly addresses research objects set forth by Vitart et al. (2012), which look to better understand the mechanism that would improve predictability of S2S weather patterns. Using joint OMI + SPV events as a forecast tool shows to better diagnose patterns of joint events, over using them separately.

- The consistency of the composited patterns increase when analyzing the joint events of the OMI + SPV. This is compared to their OMI + neutral SPV and SPV + weak OMI composites, which lacked consistency outside of regions of pattern association. North America and Asia showed increased in recurrence of the anomalous patterns, potentially leading to increased predictability of their weather patterns (Figs.3.1, 3.4, 3.5).

Through the method of significance used within this study, pattern consistency was evaluated for the composite plots (Figures 3.1, 3.5, 3.4, and 4.2). With many using the OMI + neutral SPV or the SPV + weak OMI for forecasting wintertime weather patterns, this result argues that there is increases reliability in the combined events that is not present throughout the individual events. The areas of greatest consistency for OMI + neutral SPV events were located in the North Pacific. The lack of significance throughout the NH shows

large variability in the effects of the MJO, when acting alone to influence weather patterns. Similarly the SPV + weak OMI events showed greatest consistency in the Arctic, the North Atlantic, and Europe. Variability of the patterns resulting from the SPV + neutral MJO influence was greater over Asia, the North Pacific, and North America. The OMI + neutral SPV and SPV + weak OMI shows large inconsistencies, but OMI + SPV produces patterns over these regions that decreased in their variability and increase in their reliability. Again, this shows an increase in the information gained through using the two modes in concert with one another for use in improving predictability of the patterns.

- Both OMI 2,3,4 + neutral SPV and OMI 7,8 + neutral SPV events influence the SPV. OMI 2,3,4 + neutral SPV events acted to strengthen SPV, while OMI 7,8 + neutral SPV events acted to weaken the SPV. Although the MJO influences the NAM throughout the troposphere and stratosphere, the strongest signal remains in the troposphere (Figs 4.5, 4.6).

It has been shown in various other studies that the MJO has the potential to interact with the signal of the stratosphere through wave propagation (e.g Garfinkel et al. 2012; Garfinkel and Schwartz 2017; Schwartz and Garfinkel 2017; Wang et al. 2018). Thus far, the two modes have been assumed to work independently of one another, forcing the atmospheric patterns on their own. However, this not necessarily the case and it is important to understand how the MJO influences the SPV to impact these patterns. EP-flux and its divergence (Fig. 4.4) show that there is modulation of upward wave propagation into the stratosphere by the MJO. OMI 2,3,4 appear to interfere with the patterns as to disallow anomalous wave propagation into the stratosphere. OMI 7,8, on the other hand, show anomalously strong vertical wave propagation, impacting not only OMI + neutral SPV cases, but joint cases as well. Further investigating the stratospheric response to MJO convection(Fig. 4.5, 4.6), anomalous changes in the NAM patterns and EP-flux divergence, both in the stratosphere and troposphere, are observed to be influenced by changes in the MJO convection. The OMI 2,3,4 favors a more positive NAM, while OMI 7,8 produced a weakened NAM state

in the troposphere, lagged by changes in the stratosphere. These vertical changes in NAM index throughout the atmosphere, although lagged were still relatively rapid. These results differ from those of Garfinkel et al. (2012), Garfinkel and Schwartz (2017), and Schwartz and Garfinkel (2017), that found stratosphere to troposphere pattern progression. Once the anomalous NAM signal occurs within the stratosphere, the residence time is relatively short compared to that of an initiated SPV event. Here it is not found that MJO initiates full SPV events with strong consistency. These result show that the MJO (in the +10-14 day lag composites) influences patterns via the troposphere, not down through the stratosphere. With the lack of strong signal from the stratosphere down to the troposphere, it cannot be concluded that the MJO works through the stratosphere to influence tropospheric patterns. There is still more analysis that needs to be completed to be able to resolve the MJO's influence on longer timescale events. However, here it is not shown that OMI 2,3,4 initiates strong SPV events and OMI 7,8 initiates weak SPV events.

However, the combined events of the OMI 7,8 + SPV act to impact the current SPV state. Figures 4.4g,h show strong wave propagation in and out of the stratosphere. Here the OMI 7,8 + weak SPV pattern replicates the maintenance stage within Thompson et al. (2006), which shows anomalous wave forcing in the upper troposphere, with downward wave propagation from the stratosphere. These waves directed down into the troposphere allow for the weak SPV to maintain the weakened state, with no additional eddy momentum forcing present in the stratosphere. Waves propagating and converging in the stratosphere during OMI 7,8 + strong SPV act to remove westerly momentum for the stratospheric circulation, depositing easterly momentum and weakening the SPV. This again sheds light on the constructive and destructive interference patterns that are observed through the composite analysis, and why OMI phases 7 & 8 exhibit some of the strongest interference patterns.

The composite analysis used in this study was chosen to address potential non-linearities in the combined MJO/SPV cases. As discussed, there are instances of constructive and destructive interference in the composites. These cases of interference raise the question of how much of the combined influence of the MJO and the SPV is linear. A linear regression (Equation 5.1) was formed using the OMI principal component time series and the NAM 100 hPa time series. The linear regression is given as:

$$\begin{aligned} y'(\phi,\lambda,t) = & A(\phi,\lambda) * [OMI(PC2)]'(t) \\ & + B(\phi,\lambda) * [-OMI(PC1)]'(t) \\ & + C(\phi,\lambda) * [NAM_{100}]'(t) \\ & + Constant \end{aligned} \tag{5.1}$$

In this case, OMI (PC1) is negative to match the positive RMM(PC2) (Kiladis et al. 2014). Here, y' represents the observed values of the 500 hPa GPHa, and is a function time , latitude (ϕ), and longitude(λ). The linear regression coefficients (A,B,C) are the model for the associated time series and are found through this regression. These coefficients are also functions of latitude and longitude. To best construct linear replicates of the composite analysis, the linear regression was built using a lag of 15 days.

Removing the linear dependence that each time series has on the other, the residual time series (represented with prime notation) were used to find their respective linear coefficients. Figure 5.1 shows the regression of the 500 hPa geopotential heights onto each of the regression coefficients separately. By looking for key features in the projected maps of the coefficients (Figure 5.1), these patterns contain specific patterns of the MJO and the NAM. Alone, the patterns in Figure 5.1a,b show the 500 hPa GPHa patterns that correspond to the two MJO PC time series. From comparing these time series to a phase space diagram, it becomes clear that MJO phases can be linearly replicated through the addition of the A and B linear coefficient. The NAM_{100} time series coefficient (Figure 5.1c) already linearly resembles a strong SPV, based on the very negative 500 hPa GPH anomalies over the Arctic

and the positive anomalies over the mid-latitudes. The negative NAM_{100} coefficient would therefore linearly represent the weak SPV events.

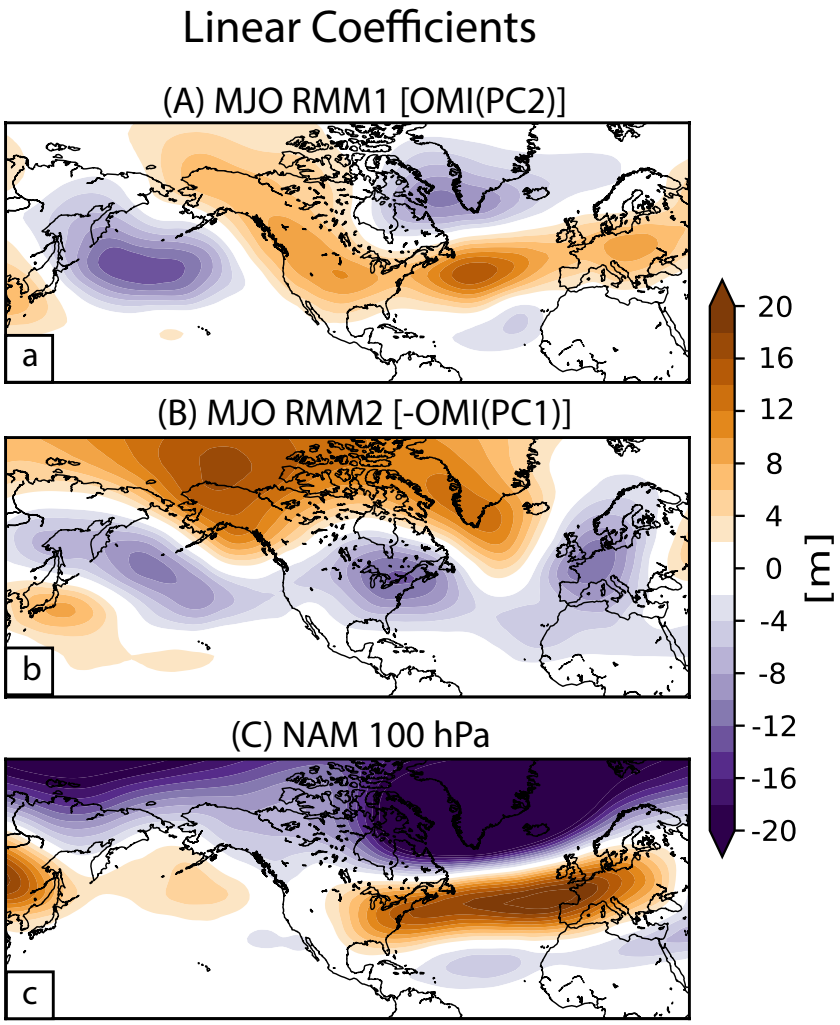

Figure 5.1: 500 hPa GPHa (m) regressed on to the linear coefficients (a) MJO RMM1 [OMI(PC2)], (b) MJO RMM2 [-OMI(PC1)], and (c) the NAM_{100} time series from Equation 5.1.

Next we replicate the joint events (i.e., different combinations of the MJO and SPV) using the linear regression coefficients in Equation 5.1. Before finding the combined events, the MJO component of the events must be constructed. This is accomplished through analyzing a phase-space diagram in Wheeler and Hendon (2004) and Kiladis et al. (2014). To build OMI phases 3 & 4, +RMM1(+OMI(PC2)) and -RMM2(OMI(PC1)) must be added

together. Conversely, to linearly construct OMI phases 7 & 8, -RMM1(-OMI(PC2)) and +RMM2(-OMI(PC1)) must be added together. To construct combined events, in Figure 5.2, these additions (Figs. 5.2a-d) are displayed with a comparison to the GPH anomaly composites for the joint events shown in Figure 3.1 (Figs. 5.2e-h). Overall, there are linear and non-linear relationships within the joint events of the MJO and SPV. First, the linearly added plots that most closely replicate the composite plots are Figs. 5.2a and 5.2d. The OMI associated signal in the Pacific combined with the SPV signal in the Arctic and the North Atlantic match very closely to the patterns of the composite analysis (Figs. 5.2e,h). Non-linearities are displayed in the linearly added plots replicating the OMI 2,3,4 + weak SPV, and OMI 7,8 + strong SPV (Figs. 5.2b,c) These plots show the Arctic as maintaining the signal of their respective SPV pattern. However, in the composite plots (Figs. 5.2f,g) this is not the case.

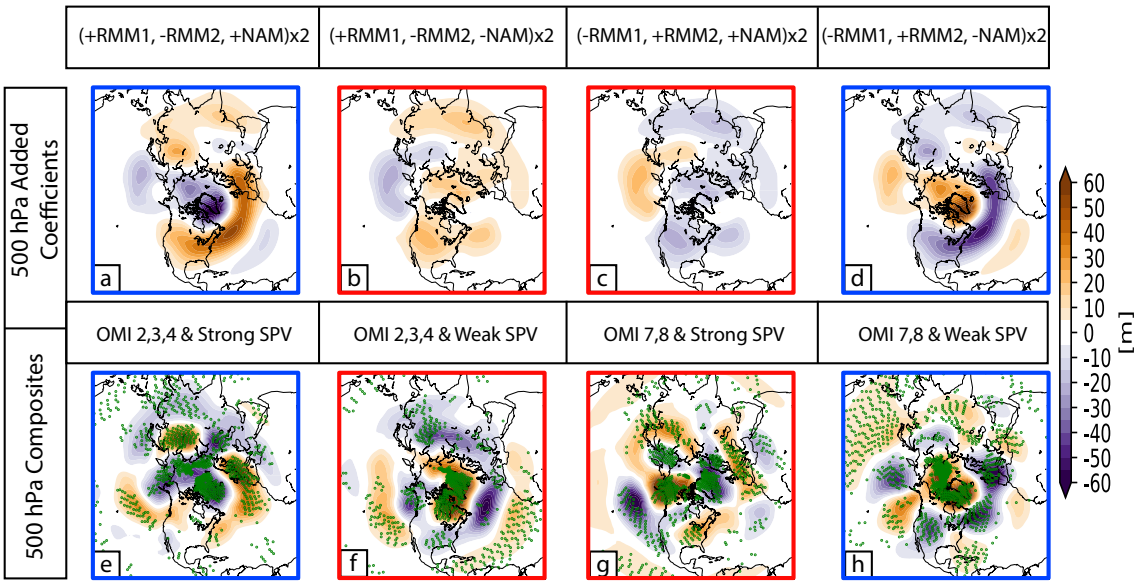

Figure 5.2: (a)-(d) 500 hPa GPHa (m) Linear regression coefficients (from Fig. 5.1) added to form composite replicates. Linearly regressed composites are doubled in amplitude to better compare to the magnitudes of the composite anomalies. (e)-(h) Same as Figure 3.1(d-e),(g-h). Linear (Blue boxes) and non-linear (Red boxes) relationships are observed.

In the linearly added coefficients there are instances of constructive Fig. 5.2a,d) and destructive (Fig. 5.2b,c) interference. Solely through linear regression the MJO and NAM indices work to produce this interference. This interference coincides with the composite analysis cases of this interference, however, additional non-linear processes are at play in the Figs. 5.2b/f, c/g. Large deviations from the linearly added coefficients show changes on the Arctic pattern, coupled by in increase in zonal wavenumber, in Fig. 5.2g. Internal interactions between the MJO and the NAM may be contributing to these non-linearities. These two modes may not work independently from one another, instead influencing the other to create the observed non-linearities.

Other tropical seasonal cycles are associated with particular weather patterns in the NH during the cold season months. El-Niño-Southern Oscillation (ENSO) is a Tropical Pacific phenomenon which most actively influences weather patterns during the NH winter, by way of influencing wave propagation (Zhang et al. 1997). Henderson and Maloney (2018) show that the MJO impacts are influenced by the state of the ENSO. Their analysis of high-latitude blocking shows that the impacts on anomalously negative North Pacific blocking frequency for phase 3 are destructive during El Niño and constructive during La Niña. Phases 7 and El Niño also constructively interfere, while phase 7 and La Niña doesn't necessarily destructively interfere with anomalously positive North Pacific blocking frequency. Our analysis, however, has not removed the influence of ENSO from the events composited, thereby including this interference of the MJO by ENSO. So, although it is beyond the scope of this study to understand the impacts that this relationship has upon the winter weather patterns in the NH, it is of interest to understand the biases within the events. Tables 5.1 and 5.2 show the number of events that occur during months that are considered using the NINO 3.4 standardized sea surface temperature (SST) anomalies. OMI 2,3,4 occurs at almost twice the frequency of OMI 7,8 during El Niño months, although potentially an artifact of sampling, Zhang (2005) finds that there is anomalous increase in western Pacific MJO activity prior to El Niño events, with very little central MJO activity in the

western-central Pacific after the event. El Niño may also cause the MJO to project on to the pattern of the third leading EOF of the OMI, which is not used to categorize the events (Kessler 2001). This frequency is seen through the combined events as well. However, during La Niña months, OMI 7,8 occurs only slightly more than OMI 2,3,4. This pattern is not continued through the joint events, as the OMI 2,3,4 joint events still occur more often. The SPV also has a slight bias to weak events during La Niña months. Of course, further subdividing our already limited sample yields even smaller sample sizes for composites. This would contribute to difficulty obtaining robust and reliable results when compositing atmospheric parameters.

Event Count During El Niño Months			
	Neut. SPV	Weak SPV	Strong SPV
Weak OMI		13	12
OMI 2,3,4	25	11	7
OMI 7,8	16	4	6

Table 5.1: Number of events for both OMI + neutral SPV, SPV + weak OMI, and combined events that occur during months where sea surface temperature anomalies of NINO 3.4 index are greater than 0.5, representing El Ninõ conditions.

5.2 Conclusion

Throughout this study, it has continually been observed that using the OMI + SPV together, allows for more consistent diagnosis of the patterns within the atmosphere +10-14 days after events. Using the OMI or the SPV individually to categorize the patterns led to inconsistencies, with large areas in the NH observing less than 66% consistency within the composite members. The growth in regions of significance is evidence that more information of the mechanisms and forcings within the atmosphere is gained through the use

Event Count During La Niña Months			
	Neut. SPV	Weak SPV	Strong SPV
Weak OMI		15	10
OMI 2,3,4	24	10	7
OMI 7,8	28	6	3

Table 5.2: Number of events for both OMI + neutral SPV, SPV+ weak OMI, and combined events that occur during months where sea surface temperature anomalies of NINO 3.4 index are less than -0.5, representing La Ninã conditions.

of both the OMI + SPV together. From these results, we argue that using the OMI + SPV together to predict winter weather patterns +10-14 days after events will result in more accurate predictions of these environments.

Composite analysis used throughout this study displayed regions where the MJO and the SPV retained a relationship with the patterns. These patterns occurred over the North Pacific for the OMI, and the North Atlantic and Europe for the SPV. Regions that gained the most consistency in the composite members for the joints events were Asia and North America. Being the regions of highest variability during the individual events, the joint events produced more consistent patterns over these regions. They represent regions that gain the most information and benefit from using both the OMI and the SPV together.

With the current paradigm for S2S forecasts considering either MJO or the SPV as a forecast tool, these results show overwhelming support for using the two in junction with one another. Winter weather resulting from these two climate modes is too important to be misrepresented and under-forecast. Large forecast errors, resulting from using either mode separately, would decrease through forecasting using the two modes together. This is particularly important for regions of large variability (North America and Asia), observed

in the independent events. Increased lead-time for forecast on the S2S time scale would lead to increased preparedness and safety for society.

5.3 Future Work

To obtain a complete understanding of the relationships between the MJO and the SPV to more accurately predict their resulting patterns, more work must be done. This study focused on reanalysis to composite events together, over the entire Northern Hemisphere. A few different methods of analysis may result in a more complete set of conclusions. First, it will be important to observe if the relationships and patterns that are observed in this analysis are reproduced in case studies. Since the objective of the research, on a large scale, is to be able to more accurately predict patterns during these environments, the interactions on a case by case basis will be most important to analyze. Investigating the frequency of composite members reproducing the anomalous pattern, this research showed that pattern consistency is gained when using joint composites of the MJO and the SPV. However, this may not be representative of individual event analysis, making it an invaluable step in furthering this research.

The results from a case study perspective will also be important for improving how models handles these relationships. Focusing on reanalysis data, the results from this study may be used for comparing to model output. It is important to first understand how the model is reproducing these patterns, to then be able to better adjust the model for more accurate predictability. This will come from a more complete analysis of wave dynamics. This study analyzed meridional wave propagation and the positioning of stationary waves, but using a three dimensional wave analysis tool from Takaya and Nakamura (2001) would show horizontal and vertical wave propagation.

Beyond the scope of this research is the effect that the state of the stratosphere has on the MJO. Frederiksen and Lin (2013) show that southeastward wave activity flux into the western Indian Ocean can initiate MJO convection in this region. Meaning that, similar to

how the MJO influences the stratosphere, the stratosphere may potentially influence wave patterns that impact the phase and amplitude of the OMI through wave propagation from high latitudes to low latitudes. Here, particular phases of the OMI may prefer to be led by certain phases of the SPV. With this analysis, increased predictability of the phase and amplitude of the OMI could come from knowing the state of the stratosphere.

Finally, putting the relationships observed and the model output into practical scenarios will provide information on the improvements it makes to winter time weather predictions on the S2S time scale. Although there is still much work to be done before reaching this step, it is the final goal of this research to provide more accurate S2S predictions of winter weather patterns in the Northern Hemisphere.

Bibliography

Austin, J. F., 1980: The blocking of middle latitude westerly winds by planetary waves. *Quart. J. R. Met. Soc.*, **106**, 327–350.

Baldwin, M. P., and T. J. Dunkerton, 1999: Propagation of the Arctic Oscillation from the stratosphere to the troposphere. *J. Geophys. Res. Atmos.*, **104 (D24)**, 30,937–30,946, doi:10.1029/1999JD900445.

Baldwin, M. P., and T. J. Dunkerton, 2001: Stratospheric harbingers of anomalous weather regimes. *Science*, **294**, 581–584, doi:10.1126/science.1063315.

Baldwin, M. P., D. B. Stephenson, D. W. J. Thompson, T. J. Dunkerton, A. J. Charlton, and A. O'Neill, 2003: Stratospheric Memory and Skill of Extended-Range Weather Forecasts. *Science*, **301**, 636–640.

Barnes, E. A., and D. L. Hartmann, 2010: Dynamical Feedbacks of the Southern Annular Mode in Winter and Summer. *J. Atmos. Sci.*, **67**, 2320 – 2330, doi:10.1175/2010JAS3385.1.

Berggren, R., B. Bolin, and C.-G. Rossby, 1949: An Aerological Study of Zonal Motion, its Perturbations and Break-down. *Tellus*, **1 (2)**, 14–37, doi:10.1111/j.2153-3490.1949.tb01257.x, URL https://onlinelibrary.wiley.com/doi/abs/10.1111/j.2153-3490.1949.tb01257.x, https://onlinelibrary.wiley.com/doi/pdf/10.1111/j.2153-3490.1949.tb01257.x.

Dee, D. P., and Coauthors, 2011: The ERA-Interim reanalysis: configuration and performance of the data assimilation system. *Q. J. R. Meteorol. Soc.*, **137**, 553–597, doi:10.1002/qj.828.

Delworth, T., and Coauthors, 2006: GFDL's CM2 global coupled climate models, part 1: Formulation and simulation characteristics. *J. Climate.*, **19**, 643–674.

Edmon Jr., H. J., B. J. Hoskins, and M. E. McIntyre, 1980: Eliassen-Palm Cross Sections for the Troposphere. *J. Atmos. Sci.*, **37**, 2600–2616.

Feldstein, S. B., 2003: The Dynamics of NAO Teleconnection Pattern Growth and Decay. *Quarterly Journal of the Royal Meteorological Society*, **129 (589)**, 901–924, doi:10.1256/qj.02.76, URL https://rmets.onlinelibrary.wiley.com/doi/abs/10.1256/qj.02.76, https://rmets.onlinelibrary.wiley.com/doi/pdf/10.1256/qj.02.76.

Frederiksen, J. S., and H. Lin, 2013: Tropical–extratropical interactions of intraseasonal oscillations. *J. Atmos. Sci.*, **70**, 3180–3197, doi:10.1175/JAS-D-12-0302.1.

Garfinkel, C. I., J. J. Benedict, and E. D. Maloney, 2014: Impact of the MJO on the boreal winter extratropical circulation. *Geophys. Res. Lett.*, **41**, 6055–6062, doi:10.1002/2014GL061094.

Garfinkel, C. I., S. B. Feldstein, D. W. Waugh, C. Yoo, and S. Lee, 2012: Observed connection between stratospheric sudden warmings and the Madden-Julian Oscillation. *Geophys. Res. Lett.*, **39**, L18 807, doi:10.1029/2012GL053144.

Garfinkel, C. I., and C. Schwartz, 2017: MJO-Related Tropical Convection Anomalies Lead to More Accurate Stratospheric Vortex Variability in Subseasonal Forecast Models. *Geophys. Res. Lett.*, **44**, 10,054–10,062, doi:10.1002/2017GL074470.

Haynes, P. H., 2005: Stratospheric Dynamics. *Annu. Rev. Fluid Mech.*, **37**, 263–293, doi:10.1146/annurev.fluid.37.061903.175710.

Haynes, P. H., C. J. Marks, M. E. McIntyre, T. G. Shepherd, and K. P. Shine, 1991: On the "Downward Control" of Extratropical Diabatic Circulations by Eddy-Induced Mean Zonal Forces. *J. Atmos. Sci.*, **48**, 651–678.

Henderson, S., E. Maloney, and E. A. Barnes, 2016: The influence of the Madden-Julian Oscillation on Northern Hemisphere winter blocking. *J. Climate*, **29**, 4597–4616, doi:10.1175/JCLI-D-15-0502.1.

Henderson, S., and E. D. Maloney, 2018: The Impact of the Madden–Julian Oscillation on High-Latitude Winter Blocking during El Niño–Southern Oscillation Events. *J. Climate*, **31**, 5293–5318, doi:10.1175/JCLI-D-17-0721.1.

Hendon, H. H., and M. L. Salby, 1994: The Life Cycle of the Madden-Julian Oscillation. *J. Atmos. Sci.*, **51 (15)**, 2225–2237.

Jiang, Z., S. B. Feldstein, and S. Lee, 2017: The relationship between the Madden-Julian Oscillation and the North Atlantic Oscillation. *Q. J. R. Meteorol. Soc.*, **143**, 240–250, doi:10.1002/qj.2917.

Kessler, W. S., 2001: EOF Representations of the Madden–Julian Oscillation and Its Connection with ENSO. *J. Climate*, **14**, 3055–3061, doi:https://doi.org/10.1175/1520-0442(2001)014⟨3055:EROTMJ⟩2.0.CO;2.

Kidston, J., A. A. Scaife, S. C. Hardiman, D. M. Mitchell, N. Butchart, M. P. Baldwin, and L. J. Gray, 2015: Stratospheric influence on tropospheric jet streams, storm tracks and surface weather. *Nature Geosci.*, **8**, 433–440, doi:10.1038/NGEO2424.

Kiladis, G. N., J. Dias, K. H. Straub, M. C. Wheeler, S. N. Tulich, K. Kikuchi, K. M. Weickmann, and M. J. Ventrice, 2014: A Comparison of OLR and Circulation-Based Indices for Tracking the MJO. *Mon. Wea. Rev.*, **142**, 1697–1715, doi:10.1175/MWR-D-13-00301.1.

L'Heureux, M. L., and R. W. Higgins, 2008: Boreal winter links between the Madden–Julian Oscillation and the Arctic Oscillation. *J. Climate*, **21**, 3040–3050, doi:10.1175/2007JCLI1955.1.

Limpasuvan, V., D. W. J. Thompson, and D. L. Hartmann, 2004: The life Cycle of the Northern Hemisphere Sudden Stratospheric Warmings. *J. Climate*, **17**, 2584–2596.

Lin, H., G. Brunet, and J. Derome, 2009: An observed connection between the North Atlantic Oscillation and the Madden–Julian Oscillation. *J. Climate*, **22**, 364–380, doi: 10.1175/2008JCLI2515.1.

Madden, R. A., and P. R. Julian, 1971: Detection of a 40–50 day oscillation in the zonal wind in the tropical Pacific. *J. Atmos. Sci.*, **28**, 702–708.

Madden, R. A., and P. R. Julian, 1972: Description of global-scale circulation cells in the tropics with a 40–50 day period. *J. Atmos. Sci.*, **29**, 1109–1123.

Madden, R. A., and P. R. Julian, 1994: Oscillation of the 40–50-Day Tropical Oscillation – A Review. *Mon. Wea. Rev.*, **122**, 814–837.

Masato, G., B. J. Hoskins, and T. Woollings, 2013a: Wave-Breaking Characteristics of Northern Hemisphere Winter Blocking: A Two-Dimensionsal Approach. *J. Climate*, **26**, 4535–4549, doi:10.1175/JCLI-D-12-00240.1.

Masato, G., B. J. Hoskins, and T. Woollings, 2013b: Winter and Summer Northern Hemisphere Blocking in CMIP5 Models. *J. Climate*, **26**, 7044–7059, doi:10.1175/JCLI-D-12-00466.1.

Masato, G., B. J. Hoskins, and T. J. Woollings, 2012: Wave-breaking characteristics of midlatitude blocking. *Q. J. R. Meteorol. Soc.*, **138**, 1285–1296, doi:10.1002/qj.990.

Matthews, A. J., B. J. Hoskins, and M. Masutani, 2004: The global response to tropical heating in the Madden–Julian Oscillation during the northern winter. *Quart. J. Roy. Meteor. Soc.*, **130**, 1991–2011, doi:10.1256/qj.02.123.

Moore, R. W., O. Martius, and T. Spengler, 2010: The modulation of the subtropical and extratropical atmosphere in the Pacific basin in response to the Madden–Julian Oscillation. *Mon. Wea. Rev.*, **138**, 2761–2779, doi:10.1175/2010MWR3194.1.

Roundy, P. E., 2012: Chapter 14: Tropical-extratropical interactions. *Intraseasonal Variability of the Atmosphere-Ocean Climate System*, **2**, 497–512.

Roundy, P. E., C. J. Schreck, and M. A. Janiga, 2009: Contributions of convectively coupled equatorial rossby waves and kelvin waves to the real-time multivariate mjo indices. *Monthly Weather Review*, **137 (1)**, 469–478, doi:10.1175/2008MWR2595.1, URL https://doi.org/10.1175/2008MWR2595.1, https://doi.org/10.1175/2008MWR2595.1.

Rui, H., and B. Wang, 1990: Development Characteristics and Dynamic Structure of Tropical Intraseasonal Convective Anomalies. *J. Atmos. Sci.*, **47 (3)**, 357–379.

Schwartz, C., and C. I. Garfinkel, 2017: Relative Roles of the MJO and the Stratospheric Variability in North Atlantic and European Winter Climate. *J. Geophys. Res. Atmos.*, **122**, 4184–4201, doi:10.1002/2016JD025829.

Straub, K. H., 2013: MJO Initiation in the Real-Time Multivariate MJO Index. *J. Climate*, **26**, 1130–1151, doi:10.1175/JCLI-D-12-00074.1.

Takaya, K., and H. Nakamura, 2001: A Formulation of Phase-Independent Wave-Activity Flux for Stationary and Migratory Quasigeostrophic Eddies on a Zonally Varying Basic Flow. *J. Atmos Sci.*, **58**, 608–627.

Thompson, D. W. J., J. C. Furtado, and T. G. Shepherd, 2006: On the Tropospheric Response to Anomalous Stratospheric Wave Drag and Radiative Heating. *J. Atmos. Sci.*, **63**, 2616–2629.

Thompson, D. W. J., and J. M. Wallace, 2000: Annular modes in the extratropical circulation. Part I: Month-to-month variability. *J. Climate*, **13**, 1000–1016.

Tibaldi, S., and F. Molteni, 1990: On the operational predictability of blocking. *Tellus*, **42A**, 343–365.

Tyrlis, E., and B. J. Hoskins, 2008a: Aspects of A Northern Hemisphere Atmospheric Blocking Climatology. *J. Atmos. Sci.*, **65**, 1638–1652, doi:10.1175/2007JAS2337.1.

Tyrlis, E., and B. J. Hoskins, 2008b: The Morphology of Northern Hemisphere Blocking. *J. Atmos. Sci.*, **65**, 1653–1665, doi:10.1175/2007JAS2338.1.

Vitart, F., A. W. Robertson, and D. L. T. Anderson, 2012: Subseasonal to Seasonal Prediction Project: Bridging the Gap Between Weather and Climate. *WMO Bull.*, **61**, 23–28, URL https://public.wmo.int/en/resources/bulletin/subseasonal-seasonal-prediction-project-bridging-gap-between-weather-and-climate.

Wang, F., W. Tian, F. Xie, J. Zhang, and Y. Han, 2018: Effect of the Madden-Julian Oscillation Occurance Frequency on the Interannual Variability of Nothern Hemisphere Stratospheric Wave Activity in Winter. *J. Climate*, doi:10.1175/JCLI-D-17-0476.1.

Waugh, D. W., A. H. Sobel, and L. M. Polvani, 2017: What is the polar vortex and how does it influence weather? *Bull. Amer. Meteor. Soc.*, **98**, 37–44, doi:10.1175/BAMS-D-15-00212.1.

Wheeler, M. C., and H. H. Hendon, 2004: An all-season real-time multivariate MJO index: Development of an index for monitoring and prediction. *Mon. Wea. Rev.*, **132**, 1917–1932.

Zhang, C., 2005: Madden-Julian Oscillation. *Rev. Geophys.*, **43**, RG2003, doi:10.1029/2004RG000158.

Zhang, Y., J. M. Wallace, and D. S. Battisti, 1997: ENSO-like Interdecadal Variability: 1900-93. *J. Climate*, **10**, 1004–1020.

Zhou, S., and A. J. Miller, 2005: The Interaction of the Madden-Julian Oscillation and the Arctic Oscillation. *J. Climate*, **18**, 143–159.